PERGAMON

International Journal of Solids and Structures 38 (2001) 6525–6558

INTERNATIONAL JOURNAL OF SOLIDS and STRUCTURES

www.elsevier.com/locate/ijsolstr

Evaluation of modal stress resultants in freely vibrating plates

C.M. Wang [a,*], Y. Xiang [b], T. Utsunomiya [c], E. Watanabe [c]

[a] *Department of Civil Engineering, National University of Singapore, Kent Ridge, Singapore 119260, Singapore*
[b] *School of Engineering and Industrial Design, University of Western Sydney, Locked Bag 1797, Penrith South DC NSW 1797, Australia*
[c] *Department of Civil Engineering, Kyoto University, Kyoto 606-8501, Japan*

Received 7 April 2000

Abstract

In the dynamic analysis of a very large floating structure (VLFS), it is crucial that the stress resultants are accurately determined for design purposes. This paper highlights some problems in obtaining accurate modal stress-resultant distributions in freely vibrating rectangular plates (for modeling box-like VLFSs) using various conventional methods. First, it is shown herein that if one adopts the classical thin plate theory and the Galerkin's method with commonly used modal functions consisting of the products of free–free beam modes, the natural boundary conditions cannot be satisfied at the free edges and the shear forces are completely erroneous, even when the eigenvalues have already converged. Second, it is shown that the problem still persists somewhat with the adoption of the more refined plate theory of Mindlin and the use of both (a) NASTRAN (that employs the finite element method) and (b) the Ritz method. The former method requires extremely fine mesh designs while the latter requires very high degrees of polynomial functions to achieve some form of satisfaction of the natural boundary conditions. Third, it is demonstrated that a modified version of the Ritz method, involving the use of a penalty functional for enforcement of the natural boundary conditions, also did not solve the problem when the plate is relatively thin. In fact, the method produces artificial stiffening to the plate. It is hoped that this paper will inspire researchers to develop an efficient technique for determining accurate stress resultants in a freely vibrating plate, apart from taking the brute force approach in having an extremely fine finite element mesh or using a very high polynomial degree.

Keywords: Modal stress; Vibrating plates; Large floating structure

1. Introduction

In a wave response analysis of a box-like very large floating structure (VLFS) as shown in Fig. 1, the structure may be modeled as a thin rectangular plate and the modal superposition method for both rigid body motions and bending modes of the plate vibrating freely in air may be used. Bending modes must be included because VLFSs, for airplane runways, typically have a large dimension in one direction (up to a

* Corresponding author. Tel.: +65-874-2157; fax: +65-779-1635.
E-mail address: cvewcm@nus.edu.sg (C.M. Wang).

0020-7683/01/$ - see front matter
PII: S0020-7683(01)00040-3

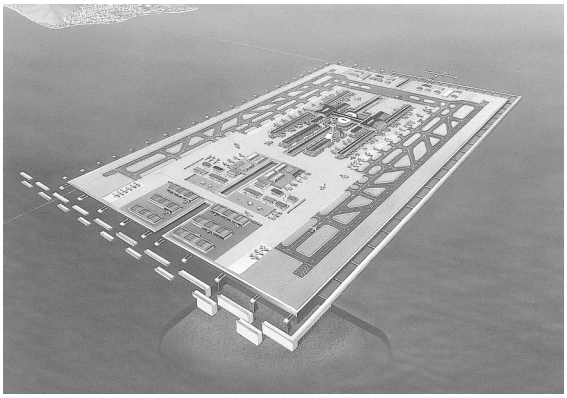

Fig. 1. Example of a VLFS (Courtesy of the Floating Structures Association of Japan).

few kilometers) and are therefore susceptible to bending deformations. Recently, dynamic response analyses on such VLFSs have been carried out by several researchers (Seto and Ochi, 1998; Nagata et al., 1998; Utsunomiya et al., 1998; Kashiwagi, 1998). Most of these vibration analyses on free rectangular thin plates used modal functions defined by the products of natural modes of free–free beams. However, when the authors checked the bending moments and shear forces distributions, it was found that these modal functions did not satisfy the natural boundary conditions at the free edges, i.e. the appropriate moments and effective shear forces did not vanish at the free edges. In the case of the effective shear forces, not only did we find nonvanishing shear forces at the edges but also entire shapes of the shear force distributions were completely erroneous as will be shown herein. The inaccuracy of the shear force distributions is primarily due to the shear forces of thin plate theory being calculated from the equations of motions.

Prompted by the need to obtain good accuracy and satisfaction of the stress resultants at the free edges for dynamic analysis of VLFS, the authors turned to the more refined plate theory of Mindlin (1951). The Mindlin plate theory provides a better estimation of the stress resultants because these quantities may be evaluated from the constitutive relations that involve rotations and only the first derivatives of the displacement and rotation functions. Moreover, the Mindlin plate theory takes into consideration the effects of transverse shear deformation and rotary inertia which become significant in the higher modes of vibration and also when the incident sea waves are oblique to the VLFSs as shown by Sim and Choi (1998).

In deriving the governing eigenvalue equation of the vibrating Mindlin plates, the Ritz method was used. For convergence of results to the exact solutions, it is essential that the Ritz functions (a) are mathematically complete, (b) satisfy the geometric boundary conditions and (c) compose of an adequate large number of independent functions. There is, however, no mandatory need for the Ritz functions to satisfy the natural boundary conditions involving moments and shear forces. This is because when the Lagrangian (or the total potential energy functional in a static problem) is minimized, the equations of motion (or the equilibrium equations in the static problem) and the natural boundary conditions are supposed to be approximately satisfied. In carrying out the Ritz vibration analysis of rectangular plates with all edges free, we choose to use mathematically complete two-dimensional polynomials for approximating the transverse displacement and the rotations of the plate cross-section because such Ritz functions may be algebraically manipulated, differentiated and integrated in an exact manner for high accuracy (Xiang et al., 1995; Liew et al., 1998). Using these Ritz functions, it was observed in the case of relatively thin plates that the bending moments more or less vanished at the free edges. However, the twisting moments and the shear forces surprisingly did not, even when calculated from the sum of rotations and first derivatives of transverse displacement and using very high degrees of polynomials. One may think that if the degree of polynomial is taken to an ultra large number, the natural boundary conditions should be satisfied. But the method be-

comes painfully slow for solution, and suffers from ill conditioning at some point. In seeking out a better method, the authors tried modifying the Ritz method by introducing penalty functionals to satisfy the natural boundary conditions, a technique somewhat akin to the enforcement of elastic boundary constraints devised by Xiang et al. (1997). The modified Ritz method is shown herein to create artificial stiffening of the plate, giving rise to erroneous stress-resultant distributions when the plate is relatively thin.

In order to check the Ritz results, the authors also used the finite element software package NASTRAN to determine the stress resultants in the freely vibrating rectangular plates. A similar observation was obtained. The stress resultants, especially the twisting moments and the shear forces, did not fully satisfy the natural boundary conditions even when the mesh is quite fine due to the presence of steep gradients of these stress resultant distributions near the free edge. This drawback of finite element in finite domain problems has been pointed out by previous researchers for bending problems (for e.g. Kant and Hinton 1983).

The problem of determining accurate stress resultants in freely vibrating plates, highlighted herein, still remains to be solved. It is hoped that this paper will inspire researchers to seek an innovatively efficient method for solution, especially for arbitrarily shaped plates with free edges. The availability of such a method will be extremely useful for the dynamic analysis of VLFSs, especially in the extraction of stress resultants for design purposes.

2. Problem definition

Consider a flat, isotropic rectangular plate of length a, width b, thickness h, Young's modulus E, Poisson's ratio v, shear modulus $G = E/[2(1+v)]$ and mass density ρ (see Fig. 2). All four edges of the plate are free. The problem is to find the vibration frequencies, mode shapes and the stress-resultant distributions that satisfy the natural boundary conditions.The aforementioned problem will be tackled using different methods which will be designated as methods A to E as shown in Table 1.

3. Method A

In method A, the classical thin plate theory is adopted. By assuming free harmonic vibration of the considered rectangular plate, the Lagrangian Π is given by

$$\Pi = U - T \tag{1}$$

where the maximum strain energy functional U is given by

$$U = \frac{1}{2}\int_{-b/2}^{b/2}\int_{-a/2}^{a/2} D\left[\left(\frac{\partial^2 w}{\partial x^2}\right)^2 + \left(\frac{\partial^2 w}{\partial y^2}\right)^2 + 2v\frac{\partial^2 w}{\partial x^2}\frac{\partial^2 w}{\partial y^2} + 2(1-v)\left(\frac{\partial^2 w}{\partial x \partial y}\right)^2\right] \mathrm{d}x\,\mathrm{d}y \tag{2}$$

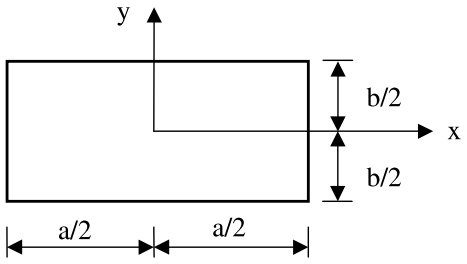

Fig. 2. Rectangular plate dimensions and coordinates system.

Table 1
Descriptions of methods A, B, C, D and E

Method	Brief descriptions of methods
A	Based on the classical thin plate theory and using the Galerkin's method with the product of $(M \times N)$ free–free beam modes as the modal function (see Utsunomiya et al. 1998).
B	Based on the Mindlin plate theory and using the Ritz method with mathematically complete two-dimensional polynomial functions of degree p to approximate the transverse displacement and rotations.
C	Based on the Mindlin plate theory and using the Ritz method with mathematically complete two-dimensional polynomial functions of degree p to approximate the transverse displacement and rotations plus a penalty functional for satisfaction of the natural boundary conditions at the free edges.
D	Based on the classical thin plate theory and using the finite element software NASTRAN.
E	Based on the Mindlin plate theory and using the finite element software NASTRAN.

and the maximum kinetic energy T is given by

$$T = \frac{1}{2}\rho h\omega^2 \int_{-b/2}^{b/2}\int_{-a/2}^{a/2} w^2 \,\mathrm{d}x\,\mathrm{d}y \tag{3}$$

in which w is the transverse displacement, $D = Eh^3/[12(1-v^2)]$ is the flexural rigidity of the plate and ω the angular frequency of the vibrating plate.

Using the Hamilton's principle, i.e.

$$\delta\Pi = 0 \tag{4}$$

one obtains

$$\begin{aligned}\int_{-b/2}^{b/2}\int_{-a/2}^{a/2}\Bigg\{D\Bigg[&\frac{\partial^2 w}{\partial x^2}\frac{\partial^2 \delta w}{\partial x^2} + \frac{\partial^2 w}{\partial y^2}\frac{\partial^2 \delta w}{\partial y^2} + v\frac{\partial^2 w}{\partial x^2}\frac{\partial^2 \delta w}{\partial y^2} + v\frac{\partial^2 w}{\partial y^2}\frac{\partial^2 \delta w}{\partial x^2}\\ &+ 2(1-v)\frac{\partial^2 w}{\partial x \partial y}\frac{\partial^2 \delta w}{\partial x \partial y}\Bigg] - \rho h\omega^2 w\,\delta w\Bigg\}\,\mathrm{d}x\,\mathrm{d}y = 0\end{aligned} \tag{5}$$

The displacement function is assumed to consist of the products of the natural modes of free–free beams:

$$w(x,y) = \sum_{m=1}^{M}\sum_{n=1}^{N}\zeta_{mn} f_m(x) g_n(y) \tag{6}$$

where ζ_{mn} is the amplitude of the mnth mode, and $f_m(x)$ and $g_n(y)$ are the modal functions of free–free beams (see Utsunomiya et al., 1998 for details of these functions).

Substituting Eq. (6) into Eq. (5) and applying the Galerkin's method, the following eigenvalue equation can be obtained

$$\sum_{m=1}^{M}\sum_{n=1}^{N}\zeta_{mn}\left(K_{mn,lj} - \omega^2 M_{mn,lj}\right) = 0 \quad (l = 1,2,\ldots,M; \quad j = 1,2,\ldots,N) \tag{7}$$

where $K_{mn,ij}$ and $M_{mn,ij}$ are the generalized stiffness and mass matrices, respectively. This eigenvalue problem may be solved using any standard eigenvalue solver.

4. Methods B and C

In method B, the Mindlin plate theory is adopted. By assuming free harmonic vibration of the considered rectangular plate, the Lagrangian Π is given by Eq. (1) where the maximum strain energy functional U is given by

$$U = \frac{1}{2}\int_{-b/2}^{b/2}\int_{-a/2}^{a/2}\left\{D\left[\left(\frac{\partial\psi_x}{\partial x}+\frac{\partial\psi_y}{\partial y}\right)^2 - 2(1-\nu)\left(\frac{\partial\psi_x}{\partial x}\frac{\partial\psi_y}{\partial y}-\frac{1}{4}\left(\frac{\partial\psi_x}{\partial y}+\frac{\partial\psi_y}{\partial x}\right)^2\right)\right] + \kappa^2 Gh\left[\left(\psi_x+\frac{\partial w}{\partial x}\right)^2+\left(\psi_y+\frac{\partial w}{\partial y}\right)^2\right]\right\}\mathrm{d}x\,\mathrm{d}y \tag{8}$$

and the maximum kinetic energy T is given by

$$T = \frac{1}{2}\rho h\omega^2\int_{-b/2}^{b/2}\int_{-a/2}^{a/2}\left[w^2+\frac{h^2}{12}\left(\psi_x^2+\psi_y^2\right)\right]\mathrm{d}x\,\mathrm{d}y \tag{9}$$

in which w is the transverse displacement, and ψ_x, ψ_y are the rotations of the plate cross-section.

In method C, we use a penalty functional to facilitate the satisfaction of the natural boundary conditions at the free edges. The augmented Lagrangian $\breve{\Pi}$ is given by

$$\breve{\Pi} = U - T + P \tag{10}$$

where the penalty functional P is defined as

$$\begin{aligned} P = \frac{1}{2}\Bigg\{ & \Lambda_s\int_{-b/2}^{b/2}\left[\left(\psi_x+\frac{\partial w}{\partial x}\right)\Big|_{x=\pm a/2}\right]^2\mathrm{d}y + \Lambda_s\int_{-a/2}^{a/2}\left[\left(\psi_y+\frac{\partial w}{\partial y}\right)\Big|_{y=\pm b/2}\right]^2\mathrm{d}x \\ & + \Lambda_b\int_{-b/2}^{b/2}\left[\left(\frac{\partial\psi_x}{\partial x}+\nu\frac{\partial\psi_y}{\partial y}\right)\Big|_{x=\pm a/2}\right]^2\mathrm{d}y + \Lambda_b\int_{-a/2}^{a/2}\left[\left(\frac{\partial\psi_y}{\partial y}+\nu\frac{\partial\psi_x}{\partial x}\right)\Big|_{y=\pm b/2}\right]^2\mathrm{d}x \\ & + \Lambda_t\int_{-b/2}^{b/2}\left[\left(\frac{\partial\psi_x}{\partial y}+\frac{\partial\psi_y}{\partial x}\right)\Big|_{x=\pm a/2}\right]^2\mathrm{d}y + \Lambda_t\int_{-a/2}^{a/2}\left[\left(\frac{\partial\psi_y}{\partial x}+\frac{\partial\psi_x}{\partial y}\right)\Big|_{y=\pm b/2}\right]^2\mathrm{d}x\Bigg\} \end{aligned} \tag{11}$$

where Λ_s, Λ_b, Λ_t are penalty multipliers which are set to some large numbers. If we set $\Lambda = 0$ in Eq. (11), we recover method B. Note that the first two terms on the right-hand side of Eq. (11) make the shear forces vanish at the edges, the next two terms for forcing the bending moments to vanish at the edges and the last two terms for the twisting moments to vanish at the edges.

For both methods B and C, we propose that the displacement functions be approximated by mathematically complete two-dimensional polynomials of degree p (Liew et al., 1998), i.e.

$$w(x,y) = \sum_{q=0}^{p}\sum_{i=0}^{q} c_m x^{q-i}y^i = \mathbf{c}^{\mathrm{T}}\phi_w, \tag{12a}$$

$$\psi_x(x,y) = \sum_{q=0}^{p}\sum_{i=0}^{q} d_m x^{q-i}y^i = \mathbf{d}^{\mathrm{T}}\phi_x, \tag{12b}$$

$$\psi_y(x,y) = \sum_{q=0}^{p}\sum_{i=0}^{q} e_m x^{q-i}y^i = \mathbf{e}^{\mathrm{T}}\phi_y \tag{12c}$$

where $m = (q+1)(q+2)/2 - i$ and c_m, d_m, e_m are the Ritz coefficients.

Applying the Ritz method,

$$\frac{\partial \breve{\Pi}}{\partial c_i} = 0, \quad \frac{\partial \breve{\Pi}}{\partial d_i} = 0, \quad \frac{\partial \breve{\Pi}}{\partial e_i} = 0, \qquad i = 1, 2, \ldots, N \tag{13}$$

where the number of polynomial terms $N = (p+1)(p+2)/2$. By substituting Eqs. (12a)–(12c) into Eq. (10) and then into Eq. (13), one obtains the eigenvalue equation given by

$$\left(\begin{bmatrix} \mathbf{K}_{cc} & \mathbf{K}_{cd} & \mathbf{K}_{ce} \\ & \mathbf{K}_{dd} & \mathbf{K}_{de} \\ \text{sym.} & & \mathbf{K}_{ee} \end{bmatrix} - \omega^2 \begin{bmatrix} \mathbf{M}_{cc} & \mathbf{M}_{cd} & \mathbf{M}_{ce} \\ & \mathbf{M}_{dd} & \mathbf{M}_{de} \\ \text{sym.} & & \mathbf{M}_{ee} \end{bmatrix} + \begin{bmatrix} \mathbf{P}_{cc} & \mathbf{P}_{cd} & \mathbf{P}_{ce} \\ & \mathbf{P}_{dd} & \mathbf{P}_{de} \\ \text{sym.} & & \mathbf{P}_{ee} \end{bmatrix} \right) \begin{Bmatrix} \mathbf{c} \\ \mathbf{d} \\ \mathbf{e} \end{Bmatrix} = 0 \tag{14}$$

where **K**s are the submatrices of the stiffness matrix, **M**s the submatrices of the mass matrix and **P**s the submatrices of the penalty matrix for the enforcement of stress resultants to vanish at the free edges.

The submatrices **K** are given by

$$\mathbf{K}_{cc} = \kappa^2 Gh \int_{-b/2}^{b/2} \int_{-a/2}^{a/2} \left(\frac{\partial \phi_w}{\partial x} \frac{\partial \phi_w^{\mathrm{T}}}{\partial x} + \frac{\partial \phi_w}{\partial y} \frac{\partial \phi_w^{\mathrm{T}}}{\partial y} \right) \mathrm{d}x\,\mathrm{d}y \tag{15a}$$

$$\mathbf{K}_{cd} = \kappa^2 Gh \int_{-b/2}^{b/2} \int_{-a/2}^{a/2} \left(\frac{\partial \phi_w}{\partial x} \phi_x^{\mathrm{T}} \right) \mathrm{d}x\,\mathrm{d}y \tag{15b}$$

$$\mathbf{K}_{ce} = \kappa^2 Gh \int_{-b/2}^{b/2} \int_{-a/2}^{a/2} \left(\frac{\partial \phi_w}{\partial y} \phi_y^{\mathrm{T}} \right) \mathrm{d}x\,\mathrm{d}y \tag{15c}$$

$$\mathbf{K}_{dd} = D \int_{-b/2}^{b/2} \int_{-a/2}^{a/2} \left(\frac{\partial \phi_x}{\partial x} \frac{\partial \phi_x^{\mathrm{T}}}{\partial x} + \frac{(1-\nu)}{2} \frac{\partial \phi_x}{\partial y} \frac{\partial \phi_x^{\mathrm{T}}}{\partial y} + \frac{\kappa^2 Gh}{D} \phi_x \phi_x^{\mathrm{T}} \right) \mathrm{d}x\,\mathrm{d}y \tag{15d}$$

$$\mathbf{K}_{de} = D \int_{-b/2}^{b/2} \int_{-a/2}^{a/2} \left(\nu \frac{\partial \phi_x}{\partial x} \frac{\partial \phi_y^{\mathrm{T}}}{\partial y} + \frac{(1-\nu)}{2} \frac{\partial \phi_x}{\partial y} \frac{\partial \phi_y^{\mathrm{T}}}{\partial x} \right) \mathrm{d}x\,\mathrm{d}y \tag{15e}$$

$$\mathbf{K}_{ee} = D \int_{-b/2}^{b/2} \int_{-a/2}^{a/2} \left(\frac{\partial \phi_y}{\partial y} \frac{\partial \phi_y^{\mathrm{T}}}{\partial y} + \frac{(1-\nu)}{2} \frac{\partial \phi_y}{\partial x} \frac{\partial \phi_y^{\mathrm{T}}}{\partial x} + \frac{\kappa^2 Gh}{D} \phi_y \phi_y^{\mathrm{T}} \right) \mathrm{d}x\,\mathrm{d}y \tag{15f}$$

The submatrices **M** are given by

$$\mathbf{M}_{cc} = \rho h \int_{-b/2}^{b/2} \int_{-a/2}^{a/2} \left(\phi_w \phi_w^{\mathrm{T}} \right) \mathrm{d}x\,\mathrm{d}y \tag{16a}$$

$$\mathbf{M}_{dd} = \frac{\rho h^3}{12} \int_{-b/2}^{b/2} \int_{-a/2}^{a/2} \left(\phi_x \phi_x^{\mathrm{T}} \right) \mathrm{d}x\,\mathrm{d}y \tag{16b}$$

$$\mathbf{M}_{ee} = \frac{\rho h^3}{12} \int_{-b/2}^{b/2} \int_{-a/2}^{a/2} \left(\phi_y \phi_y^{\mathrm{T}} \right) \mathrm{d}x\,\mathrm{d}y \tag{16c}$$

$$\mathbf{M}_{cd} = \mathbf{M}_{ce} = \mathbf{M}_{de} = 0 \tag{16d}$$

The submatrices **P** are given by

$$\mathbf{P}_{cc} = \Lambda_s \int_{-b/2}^{b/2} \left(\frac{\partial \phi_w}{\partial x} \frac{\partial \phi_w^{\mathrm{T}}}{\partial x} \right)\Big|_{x=\pm a/2} \mathrm{d}y + \Lambda_s \int_{-a/2}^{a/2} \left(\frac{\partial \phi_w}{\partial y} \frac{\partial \phi_w^{\mathrm{T}}}{\partial y} \right)\Big|_{y=\pm b/2} \mathrm{d}x \tag{17a}$$

$$\mathbf{P}_{cd} = \Lambda_s \int_{-b/2}^{b/2} \left(\frac{\partial \phi_w}{\partial x} \phi_x^{\mathrm{T}} \right)\Big|_{x=\pm a/2} \mathrm{d}y \tag{17b}$$

$$\mathbf{P}_{ce} = \Lambda_s \int_{-a/2}^{a/2} \left(\frac{\partial \phi_w}{\partial y} \phi_y^{\mathrm{T}} \right)\Big|_{y=\pm b/2} \mathrm{d}x \tag{17c}$$

$$\begin{aligned} \mathbf{P}_{dd} = {} & \Lambda_s \int_{-b/2}^{b/2} \left(\phi_x \phi_x^{\mathrm{T}} \right)\big|_{x=\pm a/2} \mathrm{d}y + \Lambda_b \int_{-b/2}^{b/2} \left(\frac{\partial \phi_x}{\partial x} \frac{\partial \phi_x^{\mathrm{T}}}{\partial x} \right)\Big|_{x=\pm a/2} \mathrm{d}y \\ & + \Lambda_b \nu^2 \int_{-a/2}^{a/2} \left(\frac{\partial \phi_x}{\partial x} \frac{\partial \phi_x^{\mathrm{T}}}{\partial x} \right)\Big|_{y=\pm b/2} \mathrm{d}x + \Lambda_t \int_{-b/2}^{b/2} \left(\frac{\partial \phi_x}{\partial y} \frac{\partial \phi_x^{\mathrm{T}}}{\partial y} \right)\Big|_{x=\pm a/2} \mathrm{d}y \\ & + \Lambda_t \int_{-a/2}^{a/2} \left(\frac{\partial \phi_x}{\partial y} \frac{\partial \phi_x^{\mathrm{T}}}{\partial y} \right)\Big|_{y=\pm b/2} \mathrm{d}x \end{aligned} \tag{17d}$$

$$\begin{aligned} \mathbf{P}_{de} = {} & \Lambda_b \nu \int_{-b/2}^{b/2} \left(\frac{\partial \phi_x}{\partial x} \frac{\partial \phi_y^{\mathrm{T}}}{\partial y} \right)\Big|_{x=\pm a/2} \mathrm{d}y + \Lambda_b \nu \int_{-a/2}^{a/2} \left(\frac{\partial \phi_x}{\partial x} \frac{\partial \phi_y^{\mathrm{T}}}{\partial y} \right)\Big|_{y=\pm b/2} \mathrm{d}x \\ & + \Lambda_t \int_{-b/2}^{b/2} \left(\frac{\partial \phi_x}{\partial y} \frac{\partial \phi_y^{\mathrm{T}}}{\partial x} \right)\Big|_{x=\pm a/2} \mathrm{d}y + \Lambda_t \int_{-a/2}^{a/2} \left(\frac{\partial \phi_x}{\partial y} \frac{\partial \phi_y^{\mathrm{T}}}{\partial x} \right)\Big|_{y=\pm b/2} \mathrm{d}x \end{aligned} \tag{17e}$$

$$\begin{aligned} \mathbf{P}_{ee} = {} & \Lambda_s \int_{-a/2}^{a/2} \left(\phi_y \phi_y^{\mathrm{T}} \right)\Big|_{y=\pm b/2} \mathrm{d}x + \Lambda_b \nu^2 \int_{-b/2}^{b/2} \left(\frac{\partial \phi_y}{\partial y} \frac{\partial \phi_y^{\mathrm{T}}}{\partial y} \right)\Big|_{x=\pm a/2} \mathrm{d}y \\ & + \Lambda_b \int_{-a/2}^{a/2} \left(\frac{\partial \phi_y}{\partial y} \frac{\partial \phi_y^{\mathrm{T}}}{\partial y} \right)\Big|_{y=\pm b/2} \mathrm{d}x + \Lambda_t \int_{-b/2}^{b/2} \left(\frac{\partial \phi_y}{\partial x} \frac{\partial \phi_y^{\mathrm{T}}}{\partial x} \right)\Big|_{x=\pm a/2} \mathrm{d}y \\ & + \Lambda_t \int_{-a/2}^{a/2} \left(\frac{\partial \phi_y}{\partial x} \frac{\partial \phi_y^{\mathrm{T}}}{\partial x} \right)\Big|_{y=\pm b/2} \mathrm{d}x \end{aligned} \tag{17f}$$

5. Methods D and E

For methods D and E, we employ the finite element software package NASTRAN. In method D, the thin shell element QUAD8 (quadrilateral eight-noded element) is used where the effect of transverse shear deformation has been neglected. In method E, the thick shell element QUAD8 with allowance for transverse shear deformation is used.

6. Vibration results

As a typical example, we consider a rectangular plate of Poisson's ratio $v = 0.3$, aspect ratio $a/b = 4$, and two different thickness-to-width ratios $h/b = 0.01$ and $h/b = 0.1$ so as to examine the influence of the plate thickness on the effectiveness of the methods used and the vibration solutions. In using the Mindlin plate theory, we have adopted a shear correction factor $\kappa^2 = 5/6$.

All five methods give rigid body motions for the first three modes. So we shall compare the vibration results for the 4th mode to the 7th mode. Tables 2–6 present partially the convergence studies of the natural frequency parameters $\Omega = \omega b^2\sqrt{\rho h/D}$ and the maximum values of the nondimensionalized modal stress resultants $\overline{M}_{xx} = M_{xx}b/D$, $\overline{M}_{yy} = M_{yy}b/D$, $\overline{M}_{xy} = M_{xy}b/D$, $\overline{Q}_x = Q_x b^2/D$, $\overline{Q}_y = Q_y b^2/D$ as computed from the five methods. These modal stress resultants have been normalized by setting $w_{\max}/b = 1$.

When using the classical thin plate theory, the frequency parameters Ω and the stress resultant parameters are independent of the thickness-to-width ratio h/b. These parameters are, however, dependent on h/b ratio when the Mindlin plate theory is used. Thus, the classical thin plate theory cannot capture the effect of the plate thickness on the natural frequency parameters and stress resultants parameters.

From the results in Tables 2–6, monotonic convergence of the natural frequencies was obtained for all five methods, except for the case of $h/b = 0.01$ and $p = 10$ of method C where we observed a missing mode of vibration. Thus, if an adequate number of terms or degrees of freedom is taken, one can be sure that the frequencies obtained are accurate. When we compare the mode shapes obtained by the five methods, they are very similar. As an example, Fig. 3a and b shows the normalized 4th mode and 5th mode, respectively. This means that method A employing the classical thin plate theory and free–free beam modal functions will suffice if the natural frequencies and the mode shapes are required in the modal superposition method for the wave response analysis of VLFSs when the plate is relatively thin.

Next, we compare the bending moment distributions as computed by methods A and B (with $h/b = 0.01$ and 0.1). Fig. 4a and b shows the normalized bending moments $\overline{M}_{xx}$ of the 4th mode and 5th mode, respectively. It can be seen that the bending moments do somewhat vanish along the edges $x = \pm a/2$ when either method A or method B is used. In the case of $\overline{M}_{yy}$, method A does not provide correct moment

Table 2
Convergence of frequency parameters Ω and maximum values of stress resultants using method A

h/b	M, N	Items	4th mode	5th mode	6th mode	7th mode
0.01 and 0.1	$M = N = 20$	Ω	1.341	3.260	3.720	6.761
		$\overline{M}_{xx}$	1.12	0.491	2.99	2.10
		$\overline{M}_{yy}$	0.337	0.239	0.897	0.887
		$\overline{M}_{xy}$	0.0659	1.06	0.391	1.97
		$\overline{Q}_x$	0.888	2.38	5.63	8.04
		$\overline{Q}_y$	9.37	3.60	24.3	15.2
0.01 and 0.1	$M = N = 30$	Ω	1.340	3.260	3.717	6.759
		$\overline{M}_{xx}$	1.12	0.477	2.99	2.15
		$\overline{M}_{yy}$	0.338	0.238	0.898	0.886
		$\overline{M}_{xy}$	0.0668	1.06	0.403	1.98
		$\overline{Q}_x$	0.883	2.84	5.71	10.0
		$\overline{Q}_y$	14.5	5.38	37.9	24.3
0.01 and 0.1	$M = N = 40$	Ω	1.340	3.260	3.715	6.759
		$\overline{M}_{xx}$	1.12	0.480	2.99	2.13
		$\overline{M}_{yy}$	0.337	0.238	0.897	0.884
		$\overline{M}_{xy}$	0.0676	1.06	0.406	1.98
		$\overline{Q}_x$	0.879	2.90	5.65	10.5
		$\overline{Q}_y$	18.8	7.59	49.5	33.8

Table 3
Convergence of frequency parameters Ω and maximum values of stress resultants using method B

h/b	Degree of polynomials, p	Items	4th mode	5th mode	6th mode	7th mode
0.01	$p=10$	Ω	1.338	3.256	3.711	6.751
		$\overline{M}_{xx}$	1.02	0.434	2.72	1.93
		$\overline{M}_{yy}$	0.0566	0.215	0.283	0.806
		$\overline{M}_{xy}$	0.0680	1.062	0.405	1.98
		$\overline{Q}_x$	5.76	98.5	35.2	179
		$\overline{Q}_y$	0.132	7.84	0.728	34.1
0.01	$p=15$	Ω	1.338	3.253	3.711	6.746
		$\overline{M}_{xx}$	1.02	0.430	2.72	1.93
		$\overline{M}_{yy}$	0.0569	0.213	0.282	0.795
		$\overline{M}_{xy}$	0.0642	1.07	0.383	1.97
		$\overline{Q}_x$	13.5	219	65.6	326
		$\overline{Q}_y$	0.164	18.6	0.759	61.8
0.01	$p=20$	Ω	1.338	3.251	3.711	6.737
		$\overline{M}_{xx}$	1.02	0.427	2.71	1.91
		$\overline{M}_{yy}$	0.0567	0.213	0.282	0.793
		$\overline{M}_{xy}$	0.0662	1.08	0.397	1.96
		$\overline{Q}_x$	18.2	282	112	513
		$\overline{Q}_y$	0.310	28.2	1.37	616
0.1	$p=10$	Ω	1.334	3.138	3.682	6.493
		$\overline{M}_{xx}$	1.02	0.382	2.67	1.71
		$\overline{M}_{yy}$	0.0517	0.155	0.265	0.566
		$\overline{M}_{xy}$	0.0514	1.06	0.302	1.94
		$\overline{Q}_x$	2.82	33.4	17.0	63.3
		$\overline{Q}_y$	0.105	6.53	0.547	27.1
0.1	$p=15$	Ω	1.334	3.137	3.682	6.488
		$\overline{M}_{xx}$	1.02	0.380	2.67	1.71
		$\overline{M}_{yy}$	0.0531	0.145	0.265	0.532
		$\overline{M}_{xy}$	0.0524	1.06	0.314	1.93
		$\overline{Q}_x$	2.90	33.7	17.7	63.7
		$\overline{Q}_y$	0.112	9.77	0.572	35.3
0.1	$p=20$	Ω	1.334	3.137	3.682	6.487
		$\overline{M}_{xx}$	1.02	0.379	2.67	1.71
		$\overline{M}_{yy}$	0.0529	0.143	0.265	0.523
		$\overline{M}_{xy}$	0.0524	1.06	0.313	1.93
		$\overline{Q}_x$	2.90	33.8	17.8	63.7
		$\overline{Q}_y$	0.109	10.2	0.551	38.0

distributions while method B gives the correct moment distribution as shown in Fig. 5a and b for the 4th mode and 5th mode, respectively and also in Tables 2 and 3.

For twisting moments, method A gives satisfactory twisting moment distributions as shown in Fig. 6a and b. Note that it is acceptable that the twisting moments do not vanish in the classical thin plate theory. For the shear forces, method A gives completely erroneous distributions as shown in Figs. 7a,b, 8a and b. Method B gives reasonably good twisting moment distribution and shear force distribution when the plate is relatively thick ($h/b = 0.1$) but displays some difficulties in satisfying the statical requirement of zero twisting moment and shear forces at the free edges when the plate is thin ($h/b = 0.01$) as shown in Figs. 6–8. The reason is due to steep gradient of the stress-resultant distributions near the plate edge. It may be possible to have vanishing twisting moments and shear forces at the edges for thin plates if a very large

Table 4
Convergence of frequency parameters Ω and maximum values of stress resultants using method C

h/b	Degree of polynomials, p	Items	4th mode	5th mode	6th mode	7th mode
0.01	$p=10$	Ω	1.349	3.784	4.943	7.635
		$\overline{M}_{xx}$	1.02	2.70	0.875	5.67
		$\overline{M}_{yy}$	0.139	0.641	1.23	2.26
		$\overline{M}_{xy}$	0.0129	0.130	1.26	0.166
		$\overline{Q}_x$	57.3	383	2003	394
		$\overline{Q}_y$	1.10	53.5	69.5	100
0.01	$p=15$	Ω	1.339	3.349	3.725	7.284
		$\overline{M}_{xx}$	1.02	0.585	2.70	2.43
		$\overline{M}_{yy}$	0.0666	0.200	0.348	1.04
		$\overline{M}_{xy}$	0.0635	1.18	0.317	2.31
		$\overline{Q}_x$	58.1	844	376	2142
		$\overline{Q}_y$	1.87	113	4.67	387
0.01	$p=20$	Ω	1.338	3.275	3.712	6.840
		$\overline{M}_{xx}$	1.02	0.485	2.71	2.06
		$\overline{M}_{yy}$	0.0609	0.181	0.292	0.694
		$\overline{M}_{xy}$	0.0692	1.16	0.413	2.23
		$\overline{Q}_x$	39.4	562	230	1089
		$\overline{Q}_y$	1.76	201	8.74	843
0.1	$p=10$	Ω	1.335	3.160	3.684	6.614
		$\overline{M}_{xx}$	1.02	0.482	2.67	1.91
		$\overline{M}_{yy}$	0.0558	0.181	0.282	0.681
		$\overline{M}_{xy}$	0.0502	1.13	0.283	2.21
		$\overline{Q}_x$	3.43	39.7	20.6	82.8
		$\overline{Q}_y$	0.145	12.9	0.964	49.7
0.1	$p=15$	Ω	1.334	3.138	3.682	6.499
		$\overline{M}_{xx}$	1.02	0.374	2.67	1.70
		$\overline{M}_{yy}$	0.0544	0.154	0.264	0.575
		$\overline{M}_{xy}$	0.0525	1.06	0.315	1.97
		$\overline{Q}_x$	2.91	33.7	17.9	65.9
		$\overline{Q}_y$	0.119	12.8	0.576	50.4
0.1	$p=20$	Ω	1.334	3.137	3.682	6.487
		$\overline{M}_{xx}$	1.02	0.383	2.67	1.72
		$\overline{M}_{yy}$	0.0531	0.143	0.265	0.524
		$\overline{M}_{xy}$	0.0524	1.06	0.313	1.93
		$\overline{Q}_x$	2.90	33.7	17.8	63.9
		$\overline{Q}_y$	0.119	10.8	0.603	39.6

degree of polynomials is taken for method B, but this poses some numerical difficulties and introduce more oscillations in the stress-resultant distributions.

In an attempt to improve on the satisfaction of the natural boundary conditions, method C that features a penalty functional was used. Based on trial tests, it was found that the best magnitudes of penalty multipliers to adopt are $\Lambda_s = 10^4 \times D$, $\Lambda_b = \Lambda_t = 10 \times D$ for $h/b = 0.1$ and $\Lambda_s = 10^6 \times D$, $\Lambda_b = \Lambda_t = 10 \times D$ for $h/b = 0.01$. Method C does force the stress resultants to satisfy the natural boundary conditions as shown in Fig. 9a and b. However for thin plates ($h/b = 0.01$), the penalty functional creates some distortions to the twisting moment and shear force distributions which is clearly observed from the results in Table 4. It still remains for researchers to improve on the method to eliminate such undesirable distortions.

Table 5
Convergence of frequency parameters Ω and maximum values of stress resultants using method D

h/b	Degrees of freedoms	Items	4th mode	5th mode	6th mode	7th mode
0.01 and 0.1	1849	Ω	1.338	3.257	3.711	6.751
		$\overline{M}_{xx}$	1.02	0.433	2.73	1.95
		$\overline{M}_{yy}$	0.0573	0.219	0.285	0.813
		$\overline{M}_{xy}$	0.0624	1.07	0.375	1.98
		$\overline{Q}_x$	2.29	25.7	14.0	48.8
		$\overline{Q}_y$	0.140	7.66	0.720	28.8
0.01 and 0.1	7153	Ω	1.338	3.258	3.711	6.753
		$\overline{M}_{xx}$	1.02	0.433	2.73	1.94
		$\overline{M}_{yy}$	0.0574	0.218	0.285	0.808
		$\overline{M}_{xy}$	0.0658	1.07	0.395	1.98
		$\overline{Q}_x$	3.95	50.9	24.1	95.7
		$\overline{Q}_y$	0.156	14.5	0.808	54.6
0.01 and 0.1	28129	Ω	1.338	3.259	3.711	6.755
		$\overline{M}_{xx}$	1.02	0.432	2.73	1.94
		$\overline{M}_{yy}$	0.0573	0.219	0.285	0.813
		$\overline{M}_{xy}$	0.0676	1.06	0.407	1.98
		$\overline{Q}_x$	7.28	102	44.2	189
		$\overline{Q}_y$	0.349	28.1	1.36	106

In order to check the correctness of the Ritz results, method D and method E involving the finite element software package NASTRAN, with thin and thick shell elements, were used to obtain the vibration results. As in method A, method D does not give satisfactory convergence of the shear forces as shown by the results presented in Table 5, even when the uniform mesh design is extremely fine (up to 28,129 degrees of freedom). Thus, it may be concluded that the classical thin plate theory cannot provide good shear force distributions. Method E (with thick shell elements) gives results similar to those obtained by method B. It is rather surprising that one needs 84,387 degrees of freedom using a uniform mesh design in order to obtain the same accuracy as the Ritz method with a total of only 693 Ritz coefficients (i.e. three times the number of terms in a degree of polynomial of $p = 20$). One may consider that the proposed Ritz method is computationally more efficient than NASTRAN in solving this particular class of plate problems. But, both these conventional methods failed to model zones with steep gradients as pointed out by Kant and Hinton (1983).

It is worth noting that the foregoing stress-resultant results show that the convergence of natural frequencies does not translate into the convergence of the stress resultants and the satisfaction of the natural boundary conditions. Instead, a better convergence criterion would be one based on the maximum values of the stress resultants so as to ensure good stress-resultant distributions and satisfaction of natural boundary conditions.

7. Conclusions

The following conclusions may be made from this study:

1. The use of the classical thin plate theory will not suffice if accurate distributions of modal stress resultants, especially twisting moments and shear forces, are required in the design of VLFSs modeled as

Table 6
Convergence of frequency parameters Ω and maximum values of stress resultants using method E

h/b	Degrees of freedoms	Items	4th mode	5th mode	6th mode	7th mode
0.01	5547	Ω	1.338	3.249	3.710	6.735
		$\overline{M}_{xx}$	1.02	0.431	2.73	1.93
		$\overline{M}_{yy}$	0.0570	0.214	0.284	0.792
		$\overline{M}_{xy}$	0.0616	1.08	0.368	1.98
		$\overline{Q}_x$	2.27	25.3	13.9	48.4
		$\overline{Q}_y$	0.128	7.59	0.659	28.5
0.01	21459	Ω	1.338	3.249	3.711	6.736
		$\overline{M}_{xx}$	1.02	0.429	2.72	1.92
		$\overline{M}_{yy}$	0.0569	0.213	0.283	0.792
		$\overline{M}_{xy}$	0.0666	1.12	0.399	2.04
		$\overline{Q}_x$	3.81	48.7	23.3	91.4
		$\overline{Q}_y$	0.142	14.0	0.724	52.4
0.01	84387	Ω	1.338	3.249	3.711	6.736
		$\overline{M}_{xx}$	1.02	0.428	2.72	1.92
		$\overline{M}_{yy}$	0.0569	0.212	0.283	0.787
		$\overline{M}_{xy}$	0.0732	1.16	0.440	2.13
		$\overline{Q}_x$	6.47	88.9	39.3	166
		$\overline{Q}_y$	0.301	24.9	1.17	93.5
0.1	5547	Ω	1.336	3.153	3.692	6.525
		$\overline{M}_{xx}$	1.02	0.378	2.68	1.71
		$\overline{M}_{yy}$	0.0529	0.152	0.265	0.560
		$\overline{M}_{xy}$	0.0592	1.07	0.353	1.95
		$\overline{Q}_x$	1.75	16.9	10.8	32.7
		$\overline{Q}_y$	0.0967	5.41	0.487	20.1
0.1	21459	Ω	1.336	3.153	3.692	6.525
		$\overline{M}_{xx}$	1.02	0.381	2.68	1.72
		$\overline{M}_{yy}$	0.0527	0.156	0.263	0.576
		$\overline{M}_{xy}$	0.0536	1.06	0.319	1.93
		$\overline{Q}_x$	2.16	23.0	13.3	43.8
		$\overline{Q}_y$	0.104	7.13	0.533	26.5
0.1	84387	Ω	1.336	3.153	3.692	6.525
		$\overline{M}_{xx}$	1.02	0.379	2.68	1.72
		$\overline{M}_{yy}$	0.0527	0.155	0.263	0.570
		$\overline{M}_{xy}$	0.0527	1.06	0.314	1.93
		$\overline{Q}_x$	2.47	27.6	15.2	52.3
		$\overline{Q}_y$	0.106	8.45	0.544	31.4

freely vibrating plates. This is an important conclusion as engineers unknowingly used the modal functions for computation of the stress resultants based on the perception that the convergence of the frequencies suffices in yielding accurate modal stress-resultant distributions.

2. It is necessary to use the Mindlin plate theory for determining stress resultants in freely vibrating plates with free edges. The correct stress-resultant distributions that satisfy the natural boundary conditions may be obtained when high degrees of polynomials are used in the Ritz method or when very fine meshes are used in the finite element method. However, when the plate is relatively thin, it is difficult to obtain converged stress resultants, especially twisting moments and shear forces because of the rapid changes of the values of these stress resultants near the free edges. It is hoped that researchers will be prompted to develop an efficient method for determining the stress resultants accurately, especially when the plate is relatively thin.

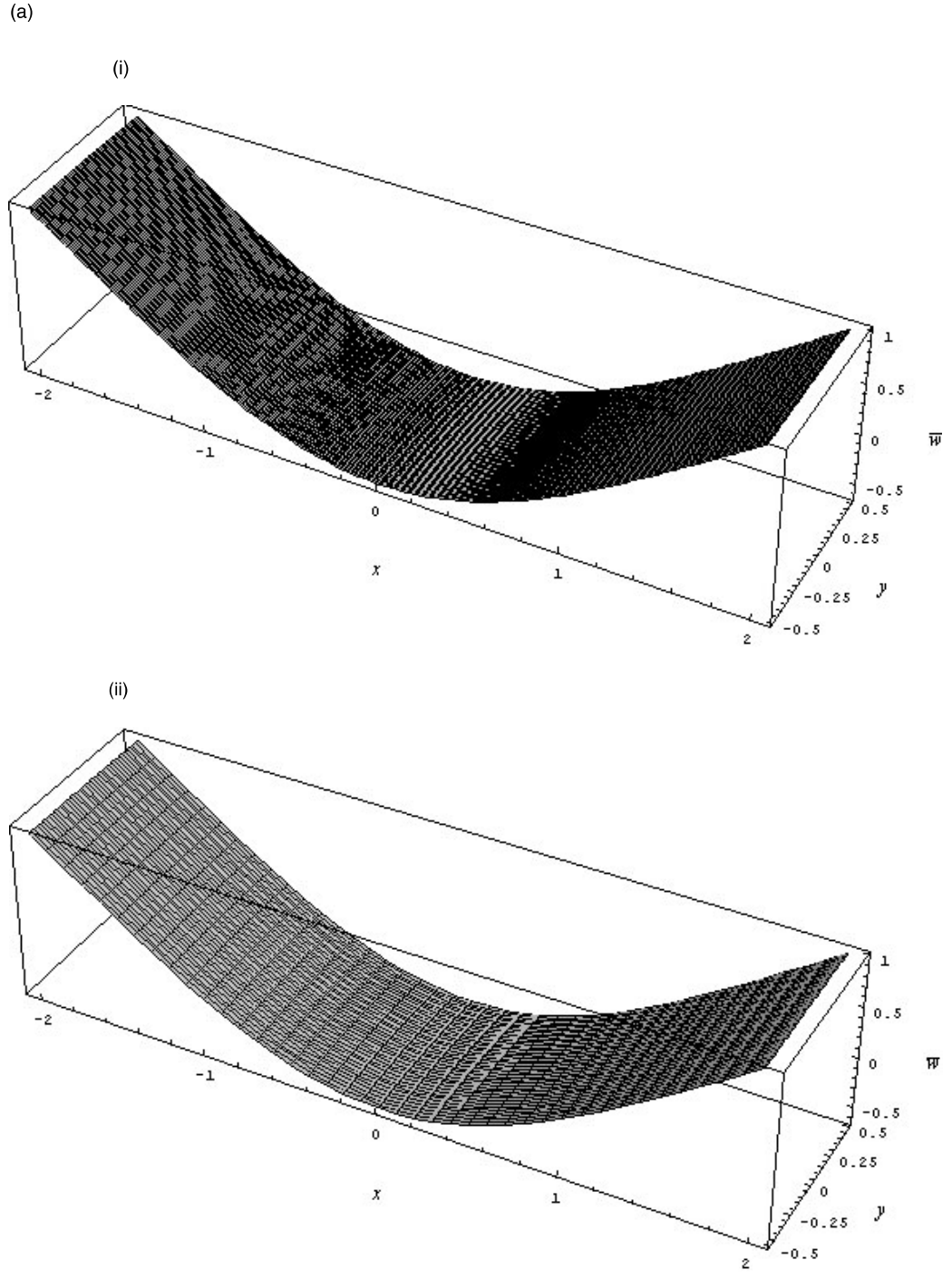

Fig. 3. (a) (i) Deflection, $\overline{w}$ for the 4th mode (method A), (ii) deflection, $\overline{w}$ for the 4th mode (method B $-$ $h/b = 0.01$); (b) (i) Deflection, $\overline{w}$ for the 5th mode (method A), (ii) deflection, $\overline{w}$ for the 5th mode (method B $-$ $h/b = 0.01$).

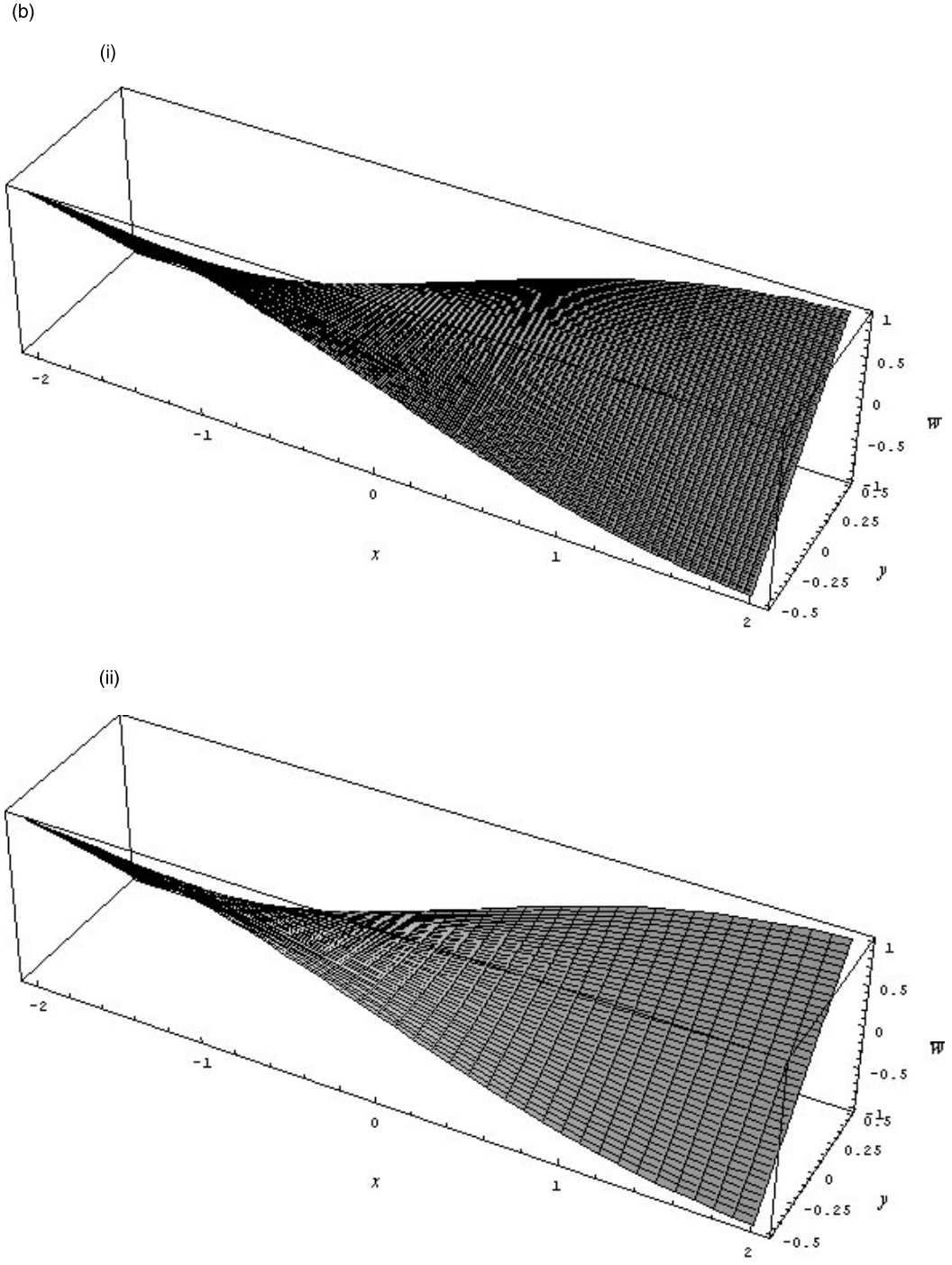

Fig. 3 (*continued*)

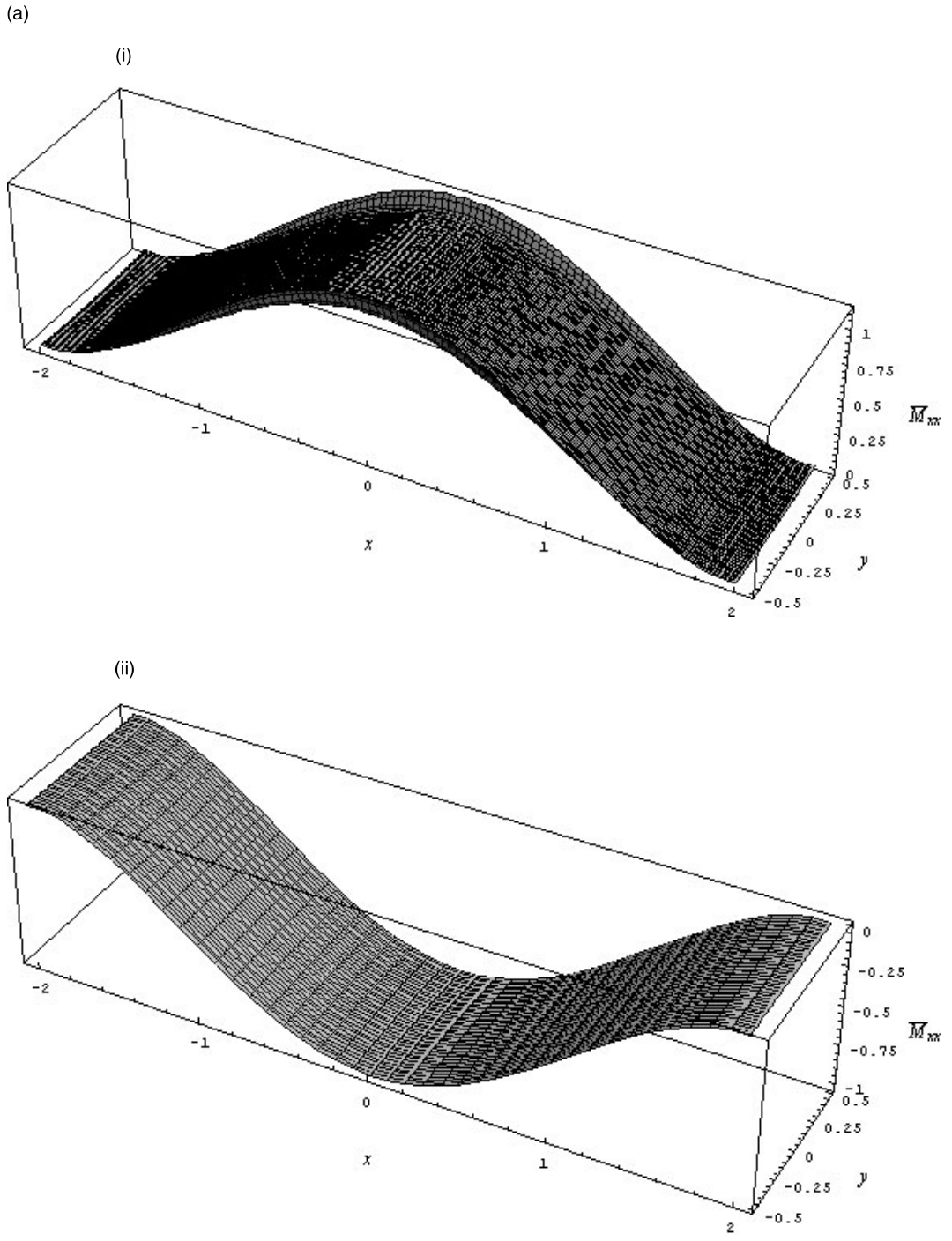

Fig. 4. (a) (i) Bending moment, $\overline{M}_{xx}$ for the 4th mode (method A), (ii) bending moment, $\overline{M}_{xx}$ for the 4th mode (method B $-$ $h/b = 0.01$), (iii) bending moment, $\overline{M}_{xx}$ for the 4th mode (method B $-$ $h/b = 0.1$); (b) (i) Bending moment, $\overline{M}_{xx}$ for the 5th mode (method A), (ii) bending moment, $\overline{M}_{xx}$ for the 5th mode (method B $-$ $h/b = 0.01$), (iii) bending moment, $\overline{M}_{xx}$ for the 5th mode (method B $-$ $h/b = 0.1$).

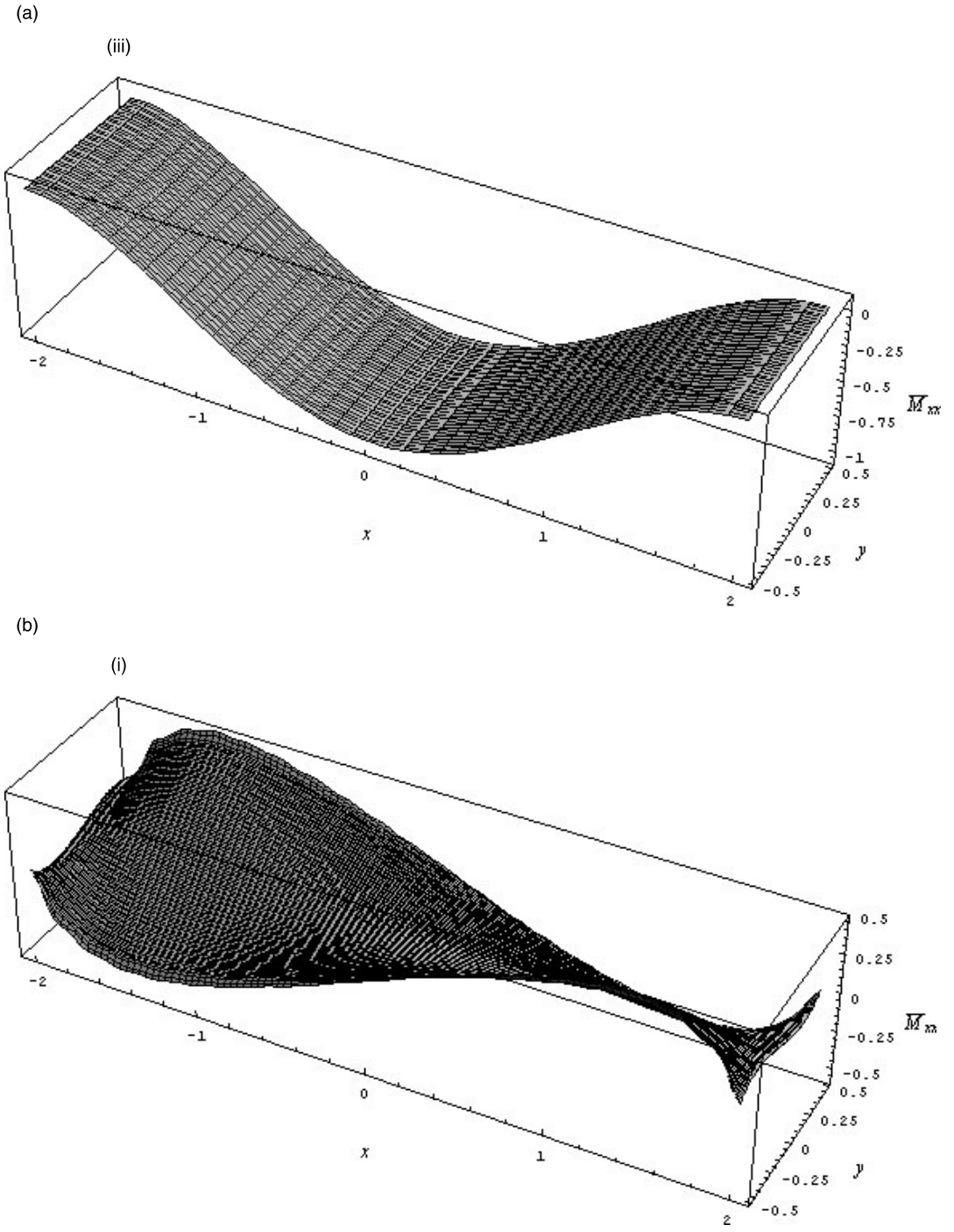

Fig. 4 (*continued*)

(b)

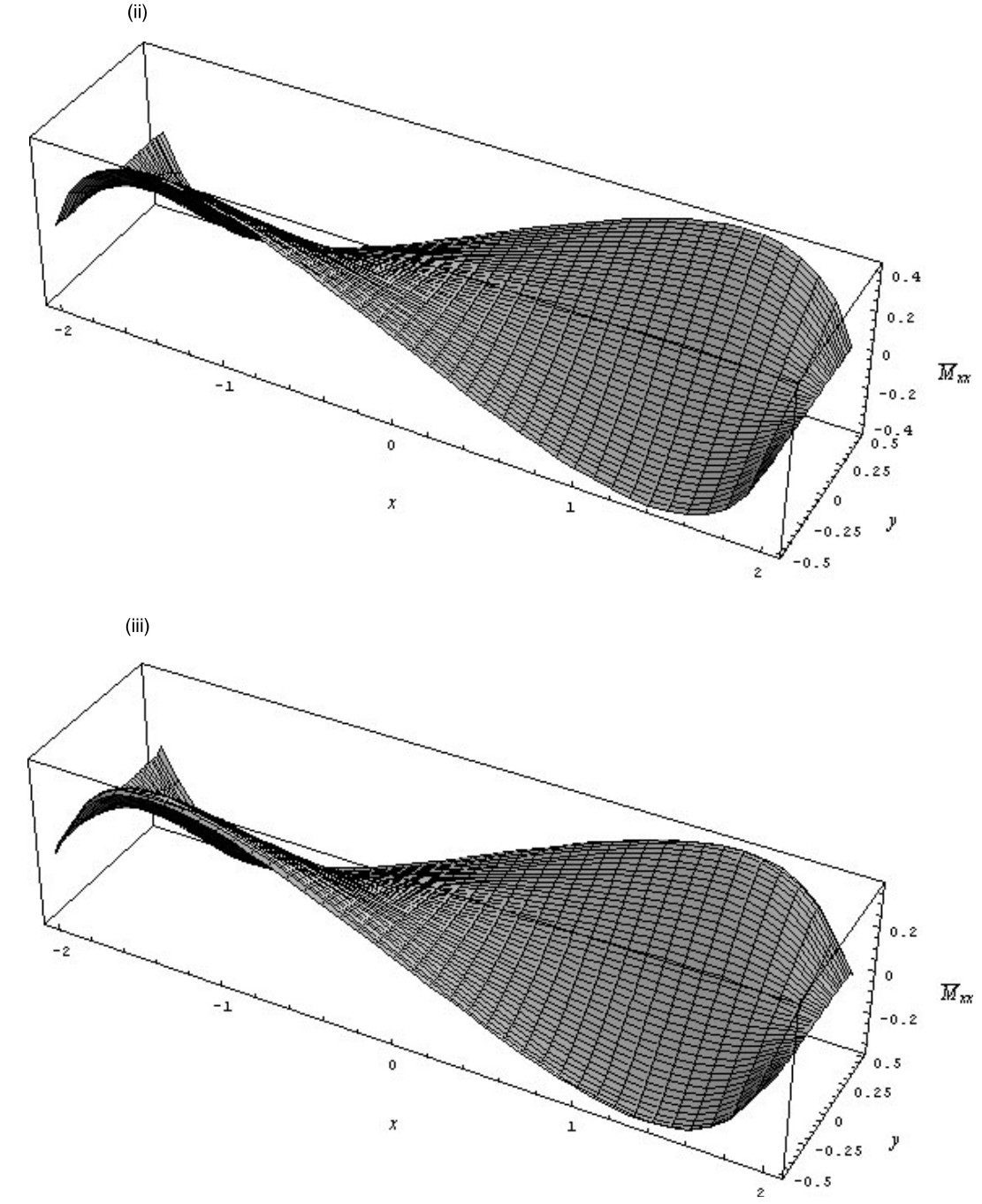

Fig. 4 (*continued*)

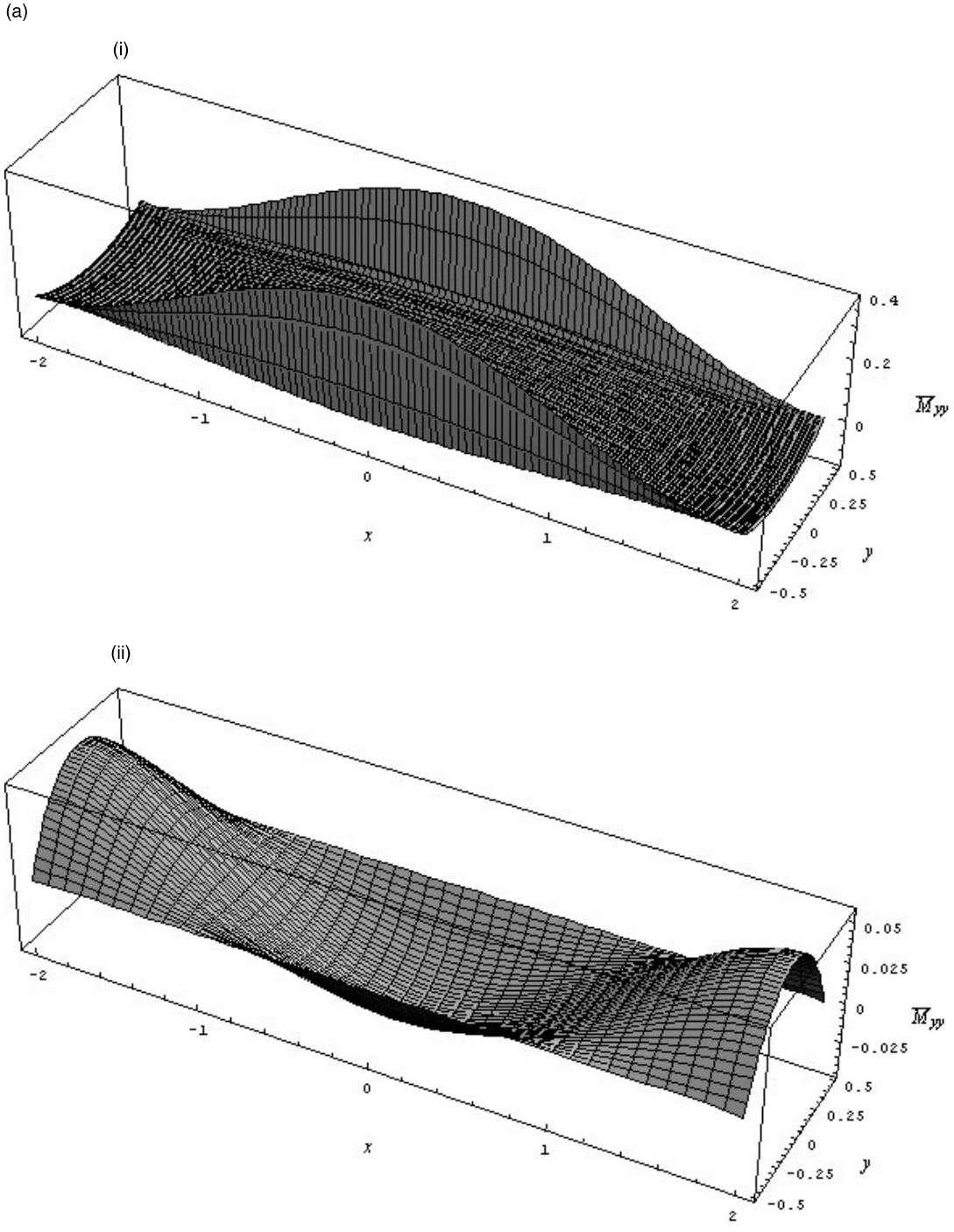

Fig. 5. (a) (i) Bending moment, $\overline{M}_{yy}$ for the 4th mode (method A), (ii) bending moment, $\overline{M}_{yy}$ for the 4th mode (method B $- h/b = 0.01$), (iii) bending moment, $\overline{M}_{yy}$ for the 4th mode (method B $- h/b = 0.1$); (b) (i) Bending moment, $\overline{M}_{yy}$ for the 5th mode (method A), (ii) bending moment, $\overline{M}_{yy}$ for the 5th mode (method B $- h/b = 0.01$), (iii) bending moment, $\overline{M}_{yy}$ for the 5th mode (method B $- h/b = 0.1$).

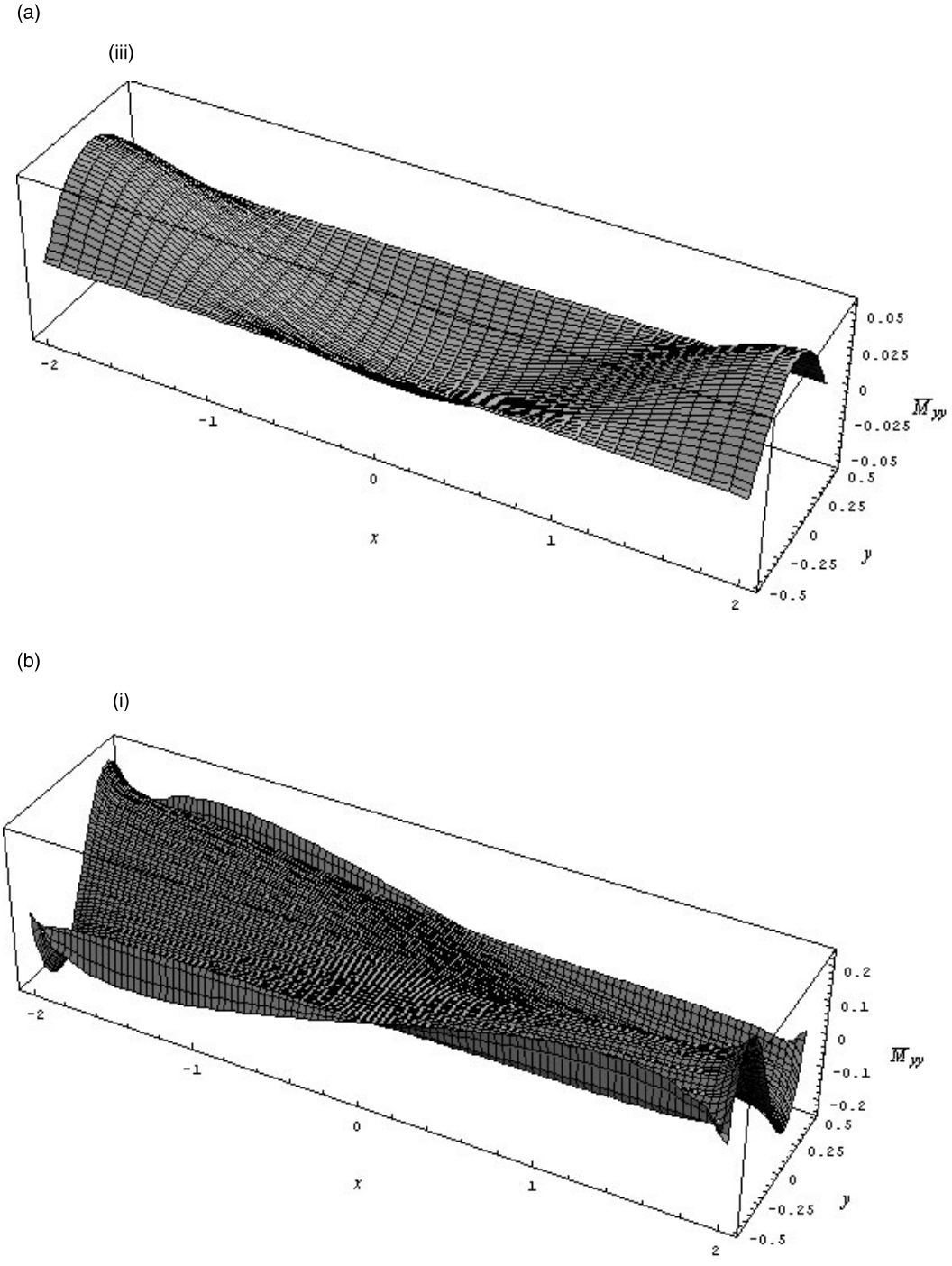

Fig. 5 (*continued*)

(b)

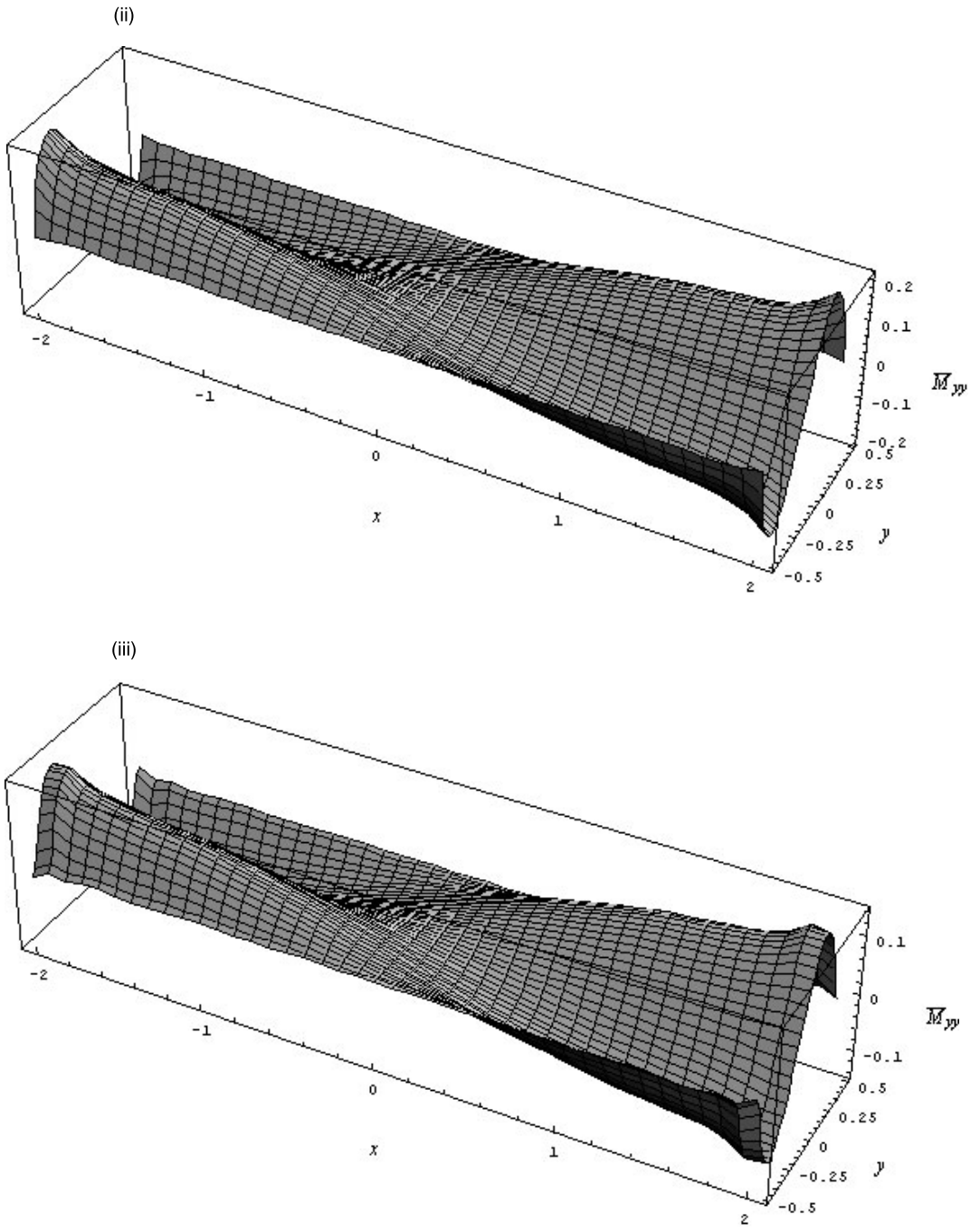

Fig. 5 (*continued*)

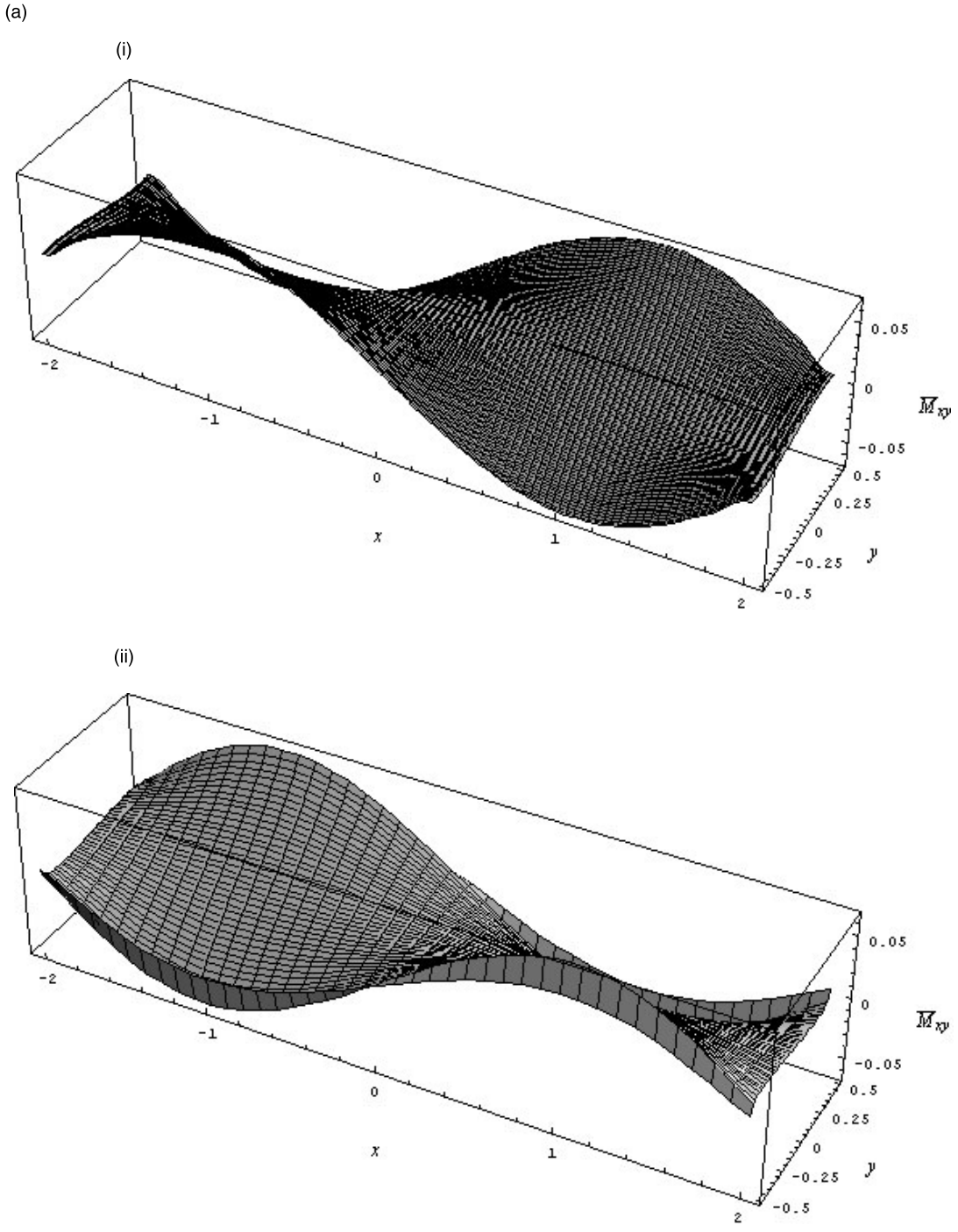

Fig. 6. (a) (i) Twisting moment, $\overline{M}_{xy}$ for the 4th mode (method A), (ii) twisting moment, $\overline{M}_{xy}$ for the 4th mode (method B $- h/b = 0.01$), (iii) twisting moment, $\overline{M}_{xy}$ for the 4th mode (method B $- h/b = 0.1$); (b) (i) Twisting moment, $\overline{M}_{xy}$ for the 5th mode (method A), (ii) twisting moment, $\overline{M}_{xy}$ for the 5th mode (method B $- h/b = 0.01$), (iii) twisting moment, $\overline{M}_{xy}$ for the 5th mode (method B $- h/b = 0.1$).

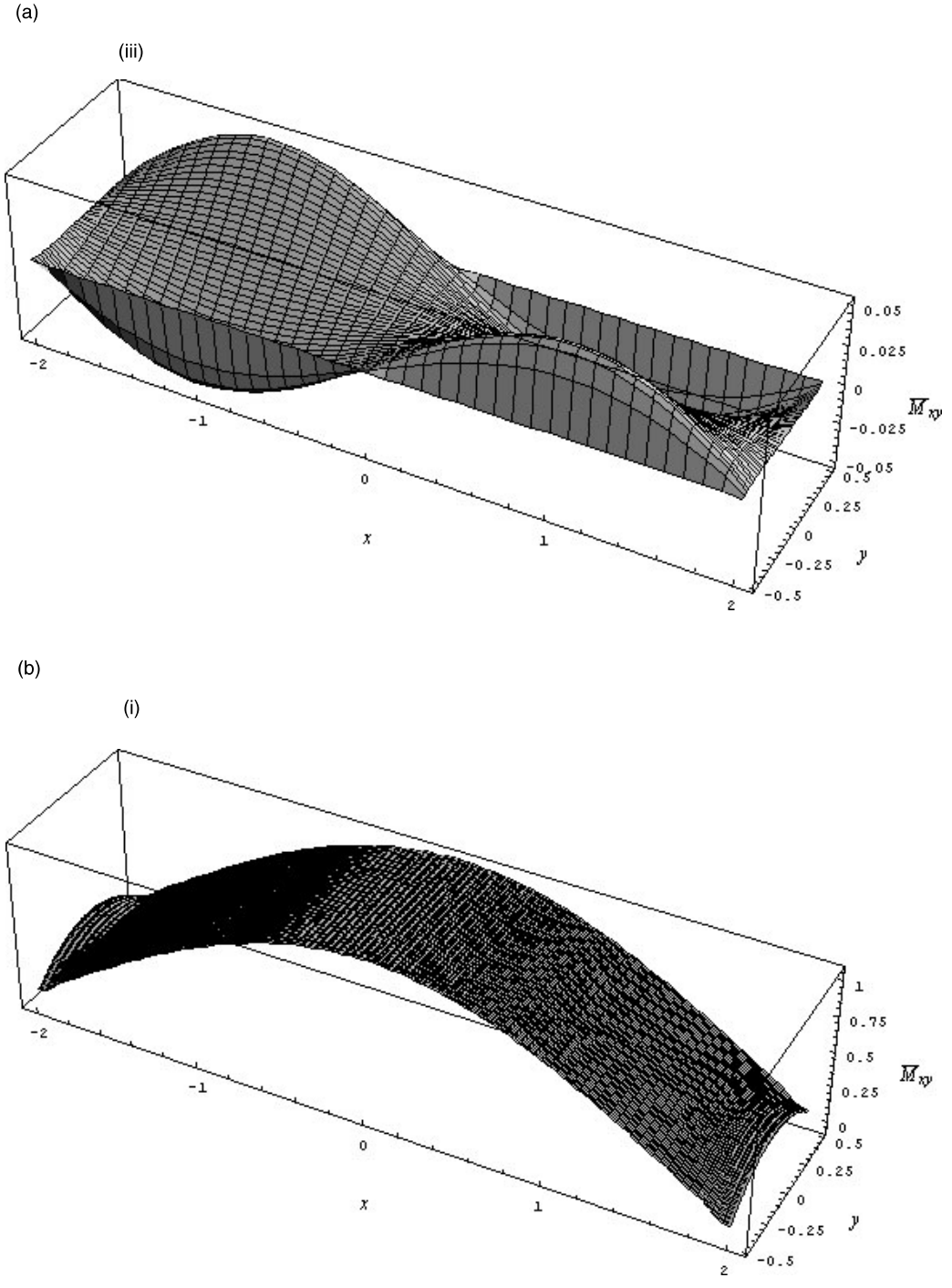

Fig. 6 (*continued*)

(b)

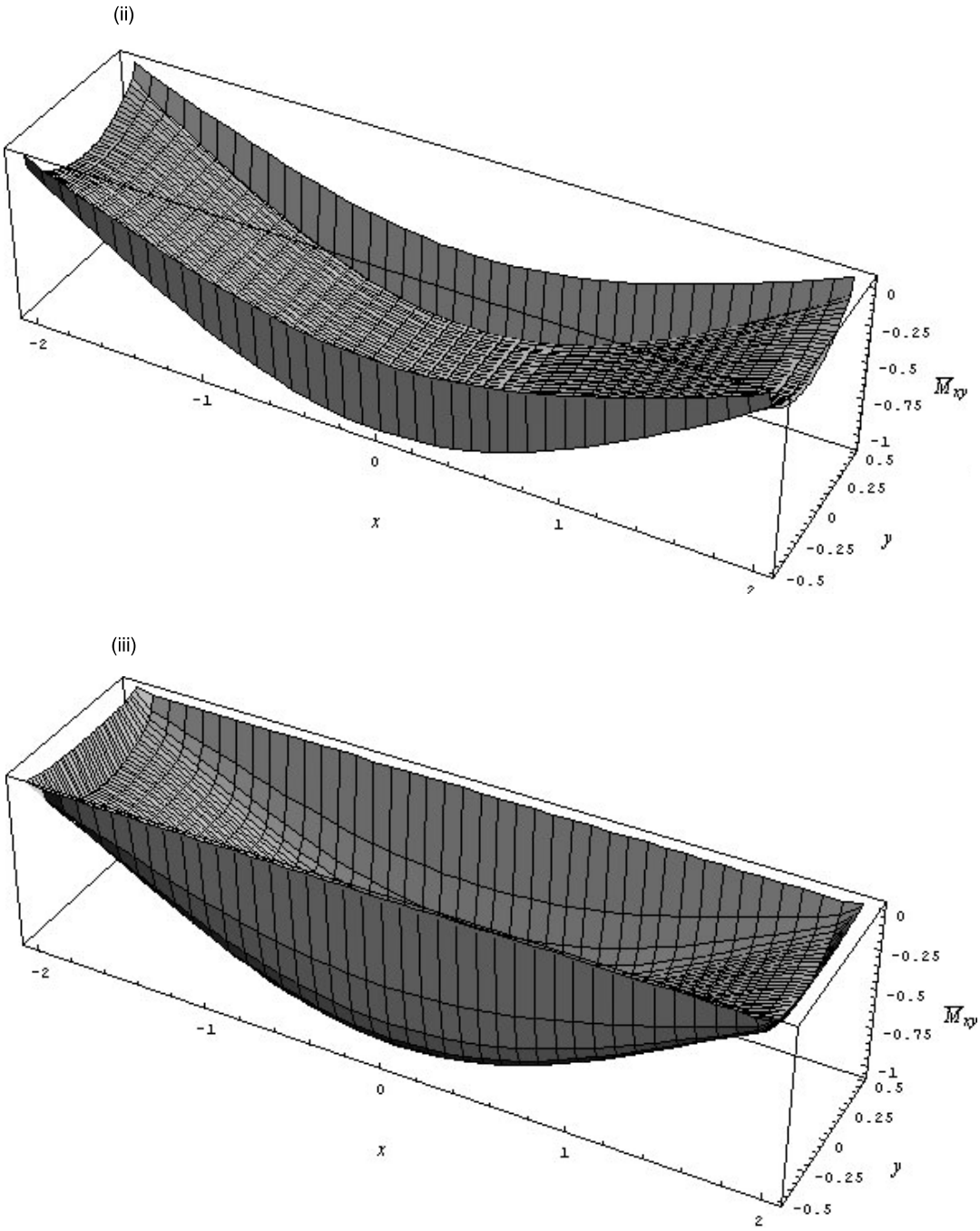

Fig. 6 (*continued*)

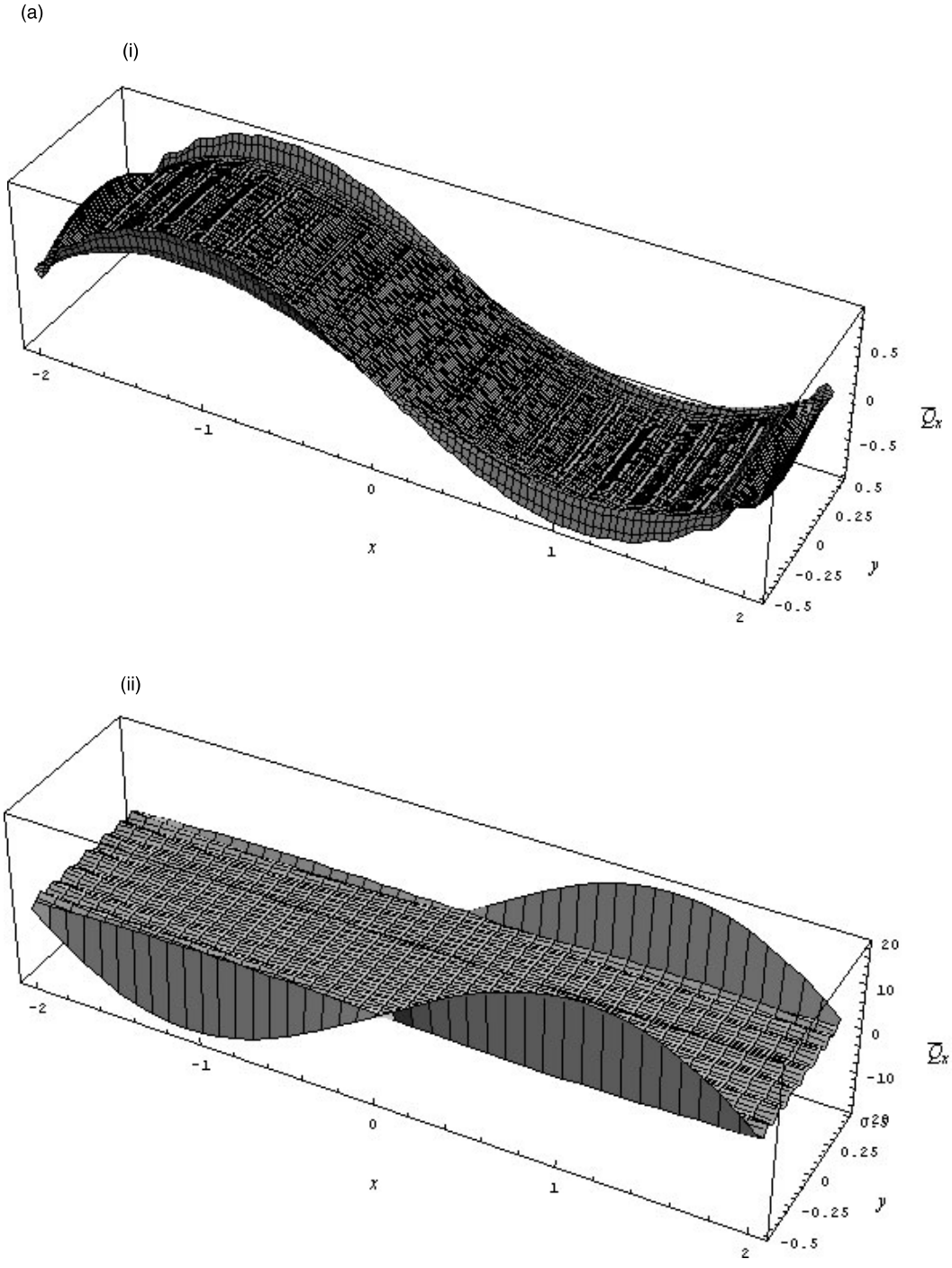

Fig. 7. (a) (i) Shear force, $\overline{Q}_x$ for the 4th mode (method A), (ii) shear force, $\overline{Q}_x$ for the 4th mode (method B $- h/b = 0.01$), (iii) shear force, $\overline{Q}_x$ for the 4th mode (method B $- h/b = 0.1$); (b) (i) Shear force, $\overline{Q}_x$ for the 5th mode (method A), (ii) shear force, $\overline{Q}_x$ for the 5th mode (method B $- h/b = 0.01$), (iii) shear force, $\overline{Q}_x$ for the 5th mode (method B $- h/b = 0.1$).

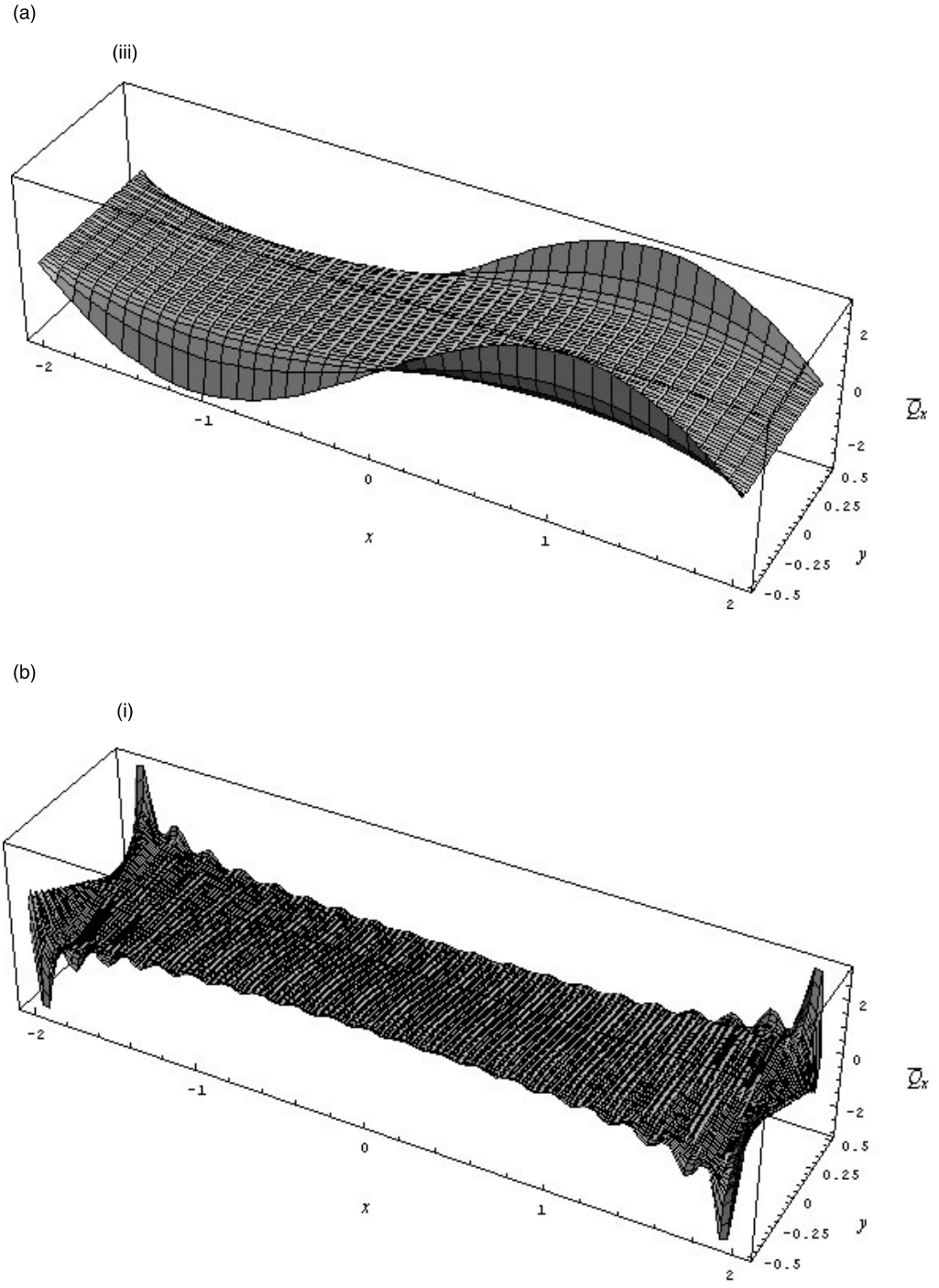

Fig. 7 (*continued*)

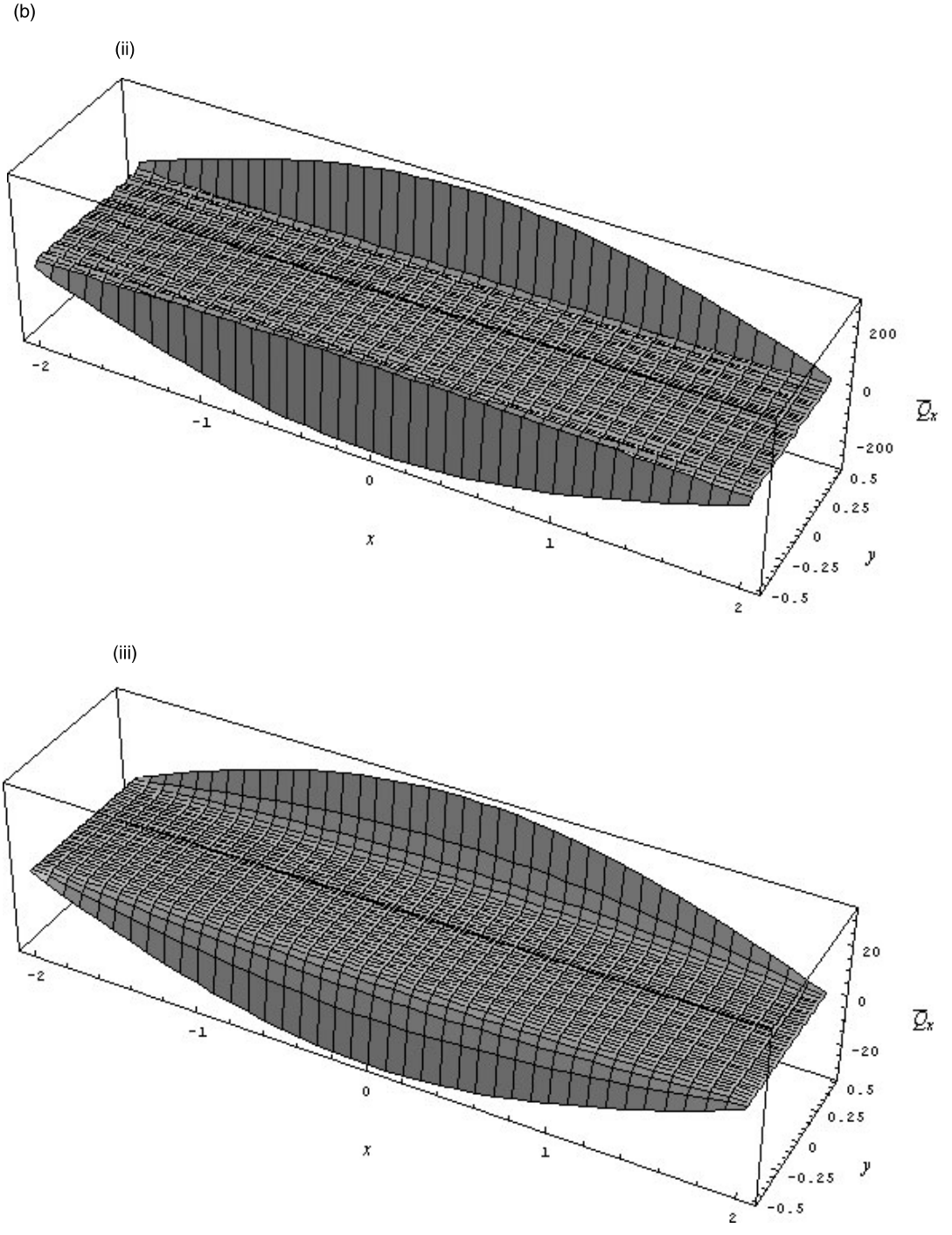

Fig. 7 (*continued*)

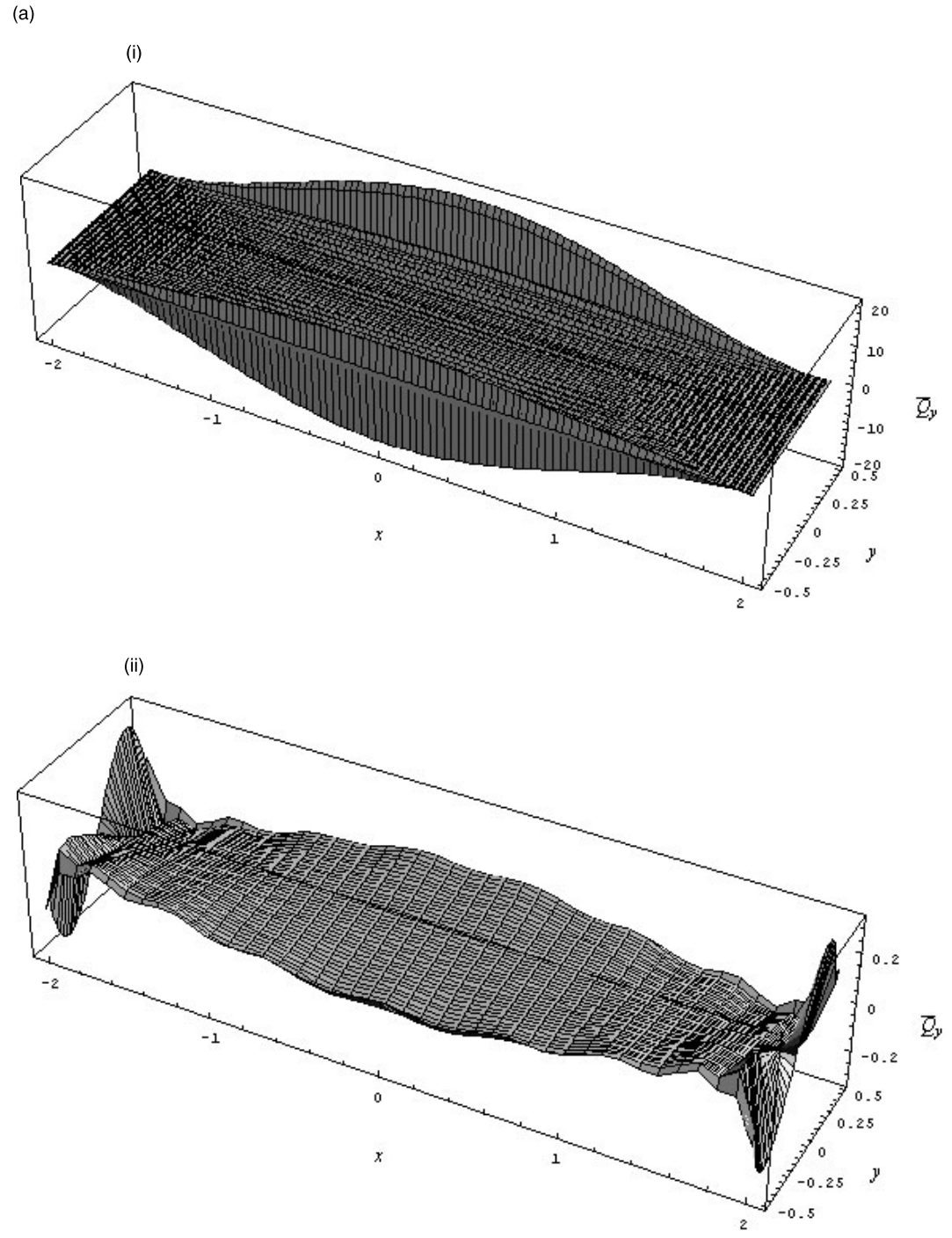

Fig. 8. (a) (i) Shear force, $\overline{Q}_y$ for the 4th mode (method A), (ii) shear force, $\overline{Q}_y$ for the 4th mode (method B $- h/b = 0.01$), (iii) shear force, $\overline{Q}_y$ for the 4th mode (method B $- h/b = 0.1$); (b) (i) Shear force, $\overline{Q}_y$ for the 5th mode (method A), (ii) shear force, $\overline{Q}_y$ for the 5th mode (method B $- h/b = 0.01$), (iii) shear force, $\overline{Q}_y$ for the 5th mode (method B $- h/b = 0.1$).

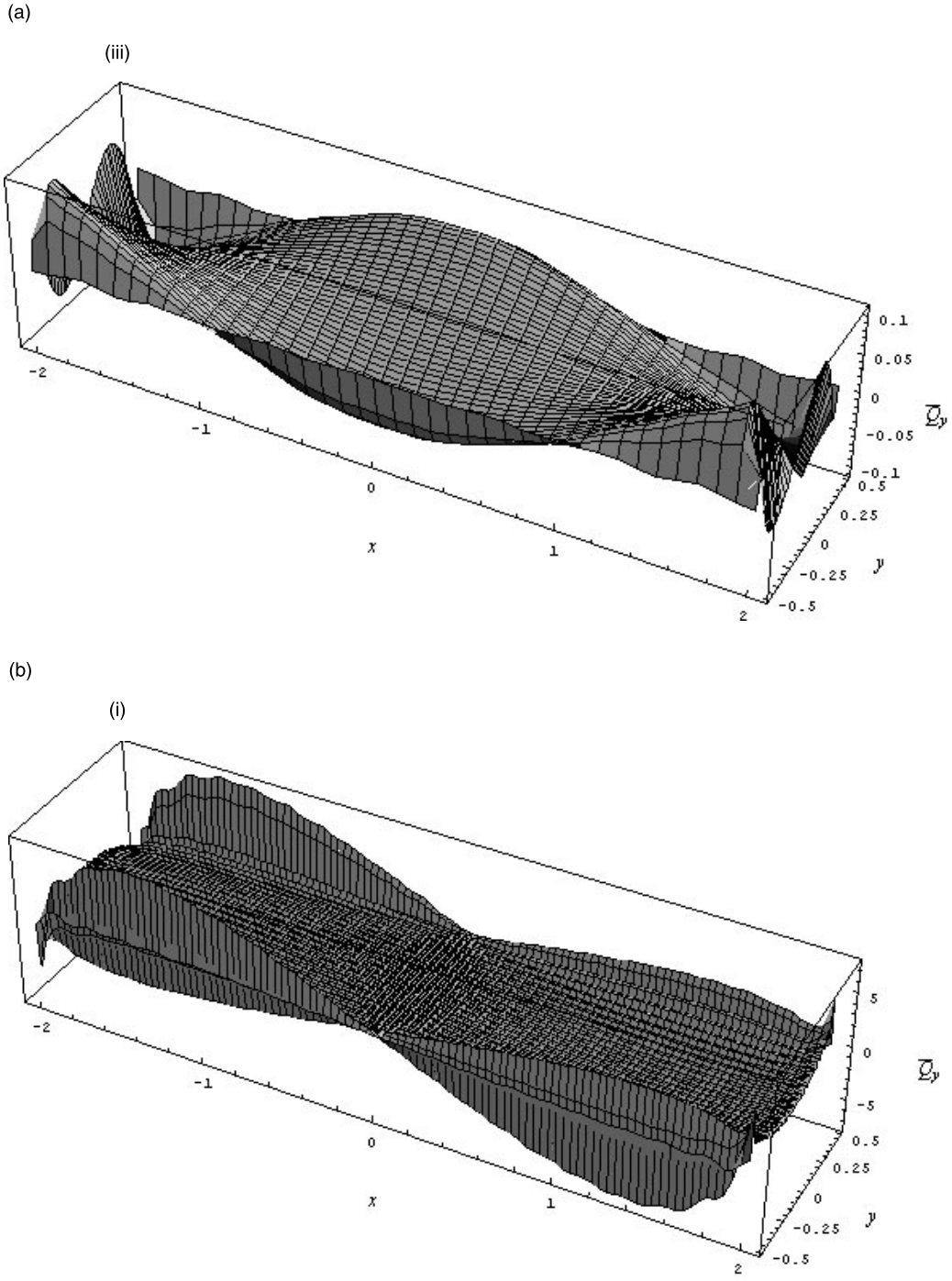

Fig. 8 (*continued*)

(b)

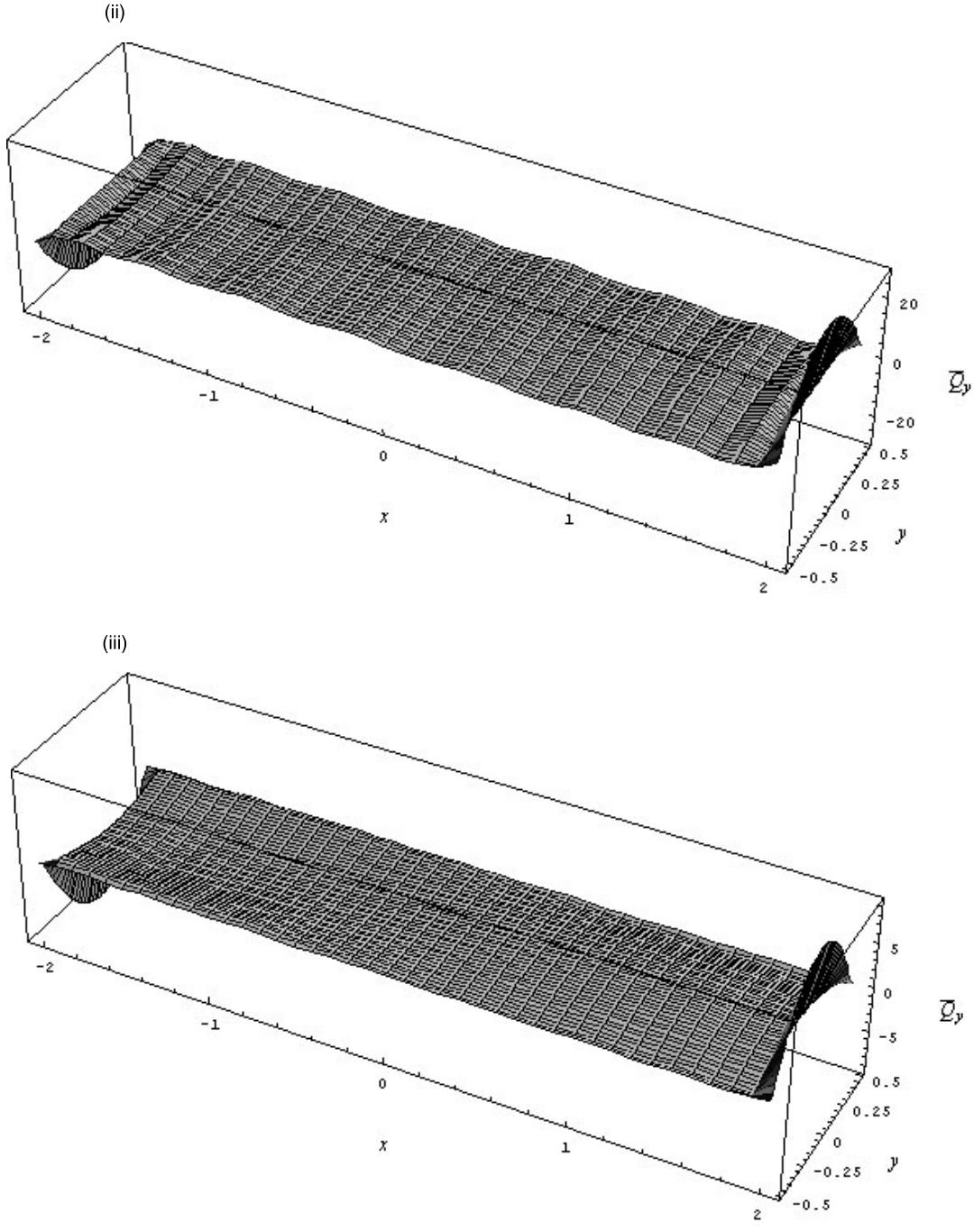

Fig. 8 (*continued*)

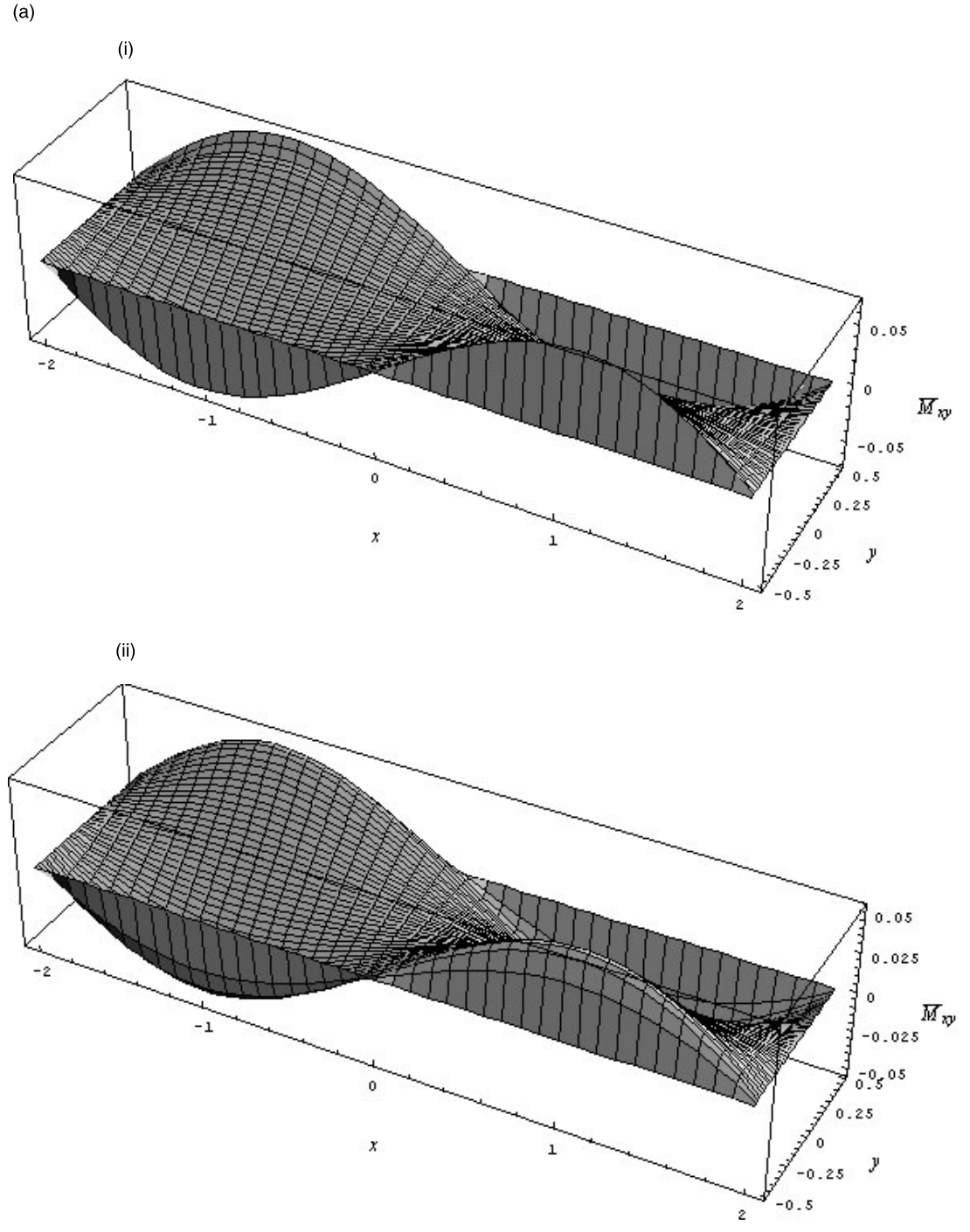

Fig. 9. (a) (i) Twisting moment, $\overline{M}_{xy}$ for the 4th mode (method C – $h/b = 0.01$), (ii) twisting moment, $\overline{M}_{xy}$ for the 4th mode (method C – $h/b = 0.1$), (iii) shear force, $\overline{Q}_x$ for the 4th mode (method C – $h/b = 0.01$), (iv) shear force, $\overline{Q}_x$ for the 4th mode (method C – $h/b = 0.1$); (b) (i) Twisting moment, $\overline{M}_{xy}$ for the 5th mode (method C – $h/b = 0.01$), (ii) twisting moment, $\overline{M}_{xy}$ for the 5th mode (method C – $h/b = 0.1$), (iii) shear force, $\overline{Q}_x$ for the 5th mode (method C – $h/b = 0.01$), (iv) shear force, $\overline{Q}_x$ for the 5th mode (method C – $h/b = 0.1$).

(a)

(iii)

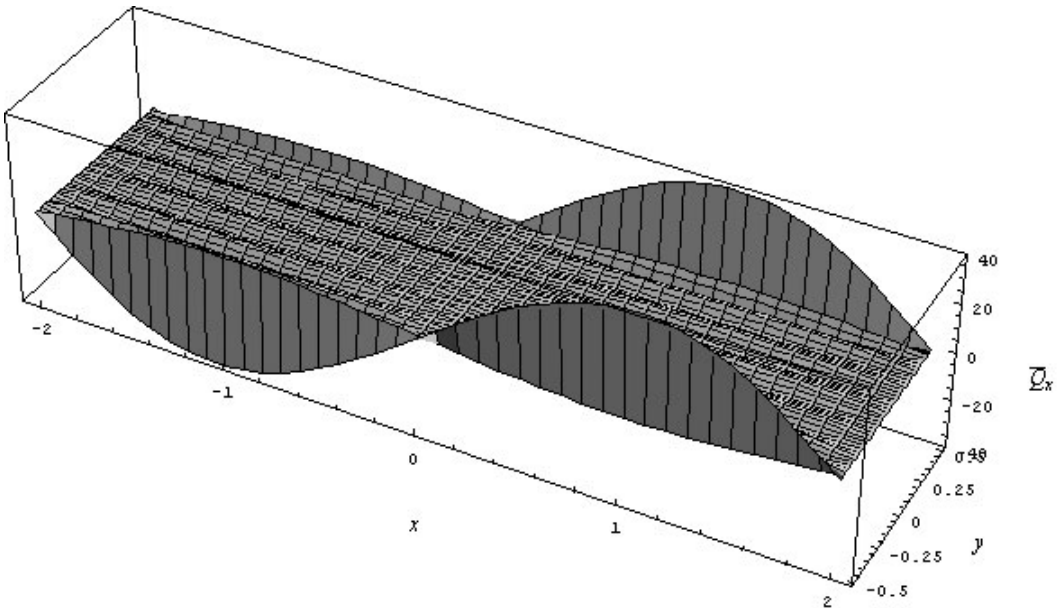

(iv)

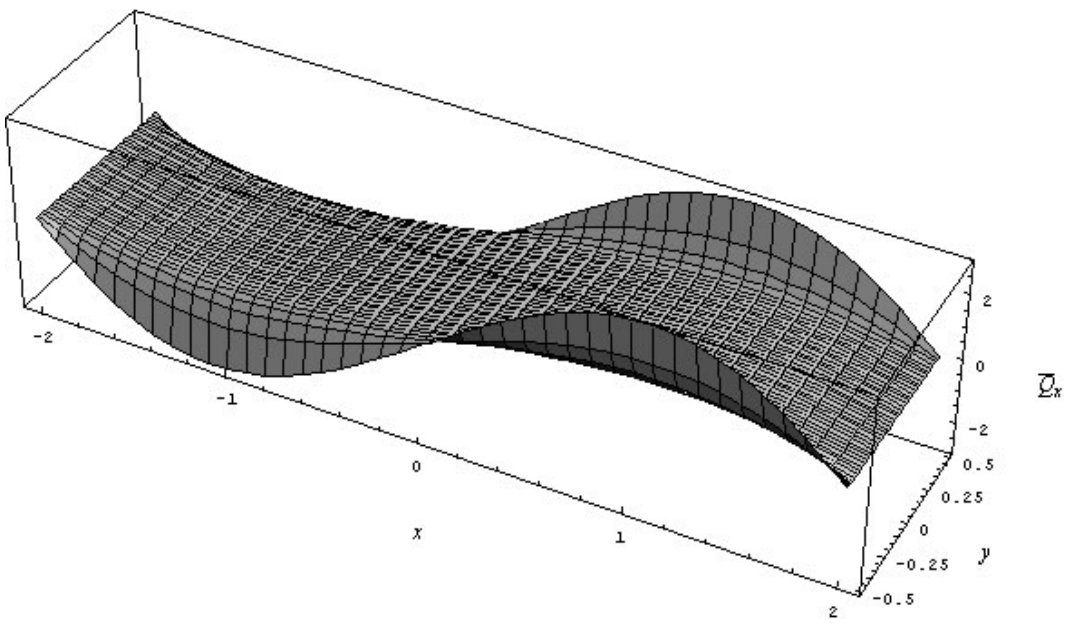

Fig. 9 (*continued*)

(b)

(i)

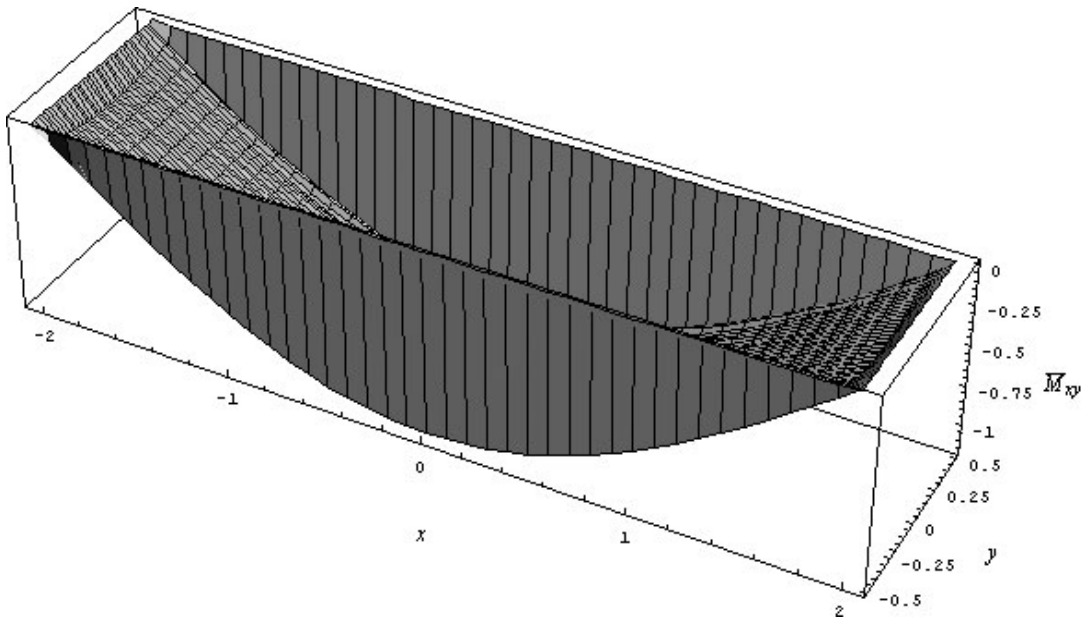

(ii)

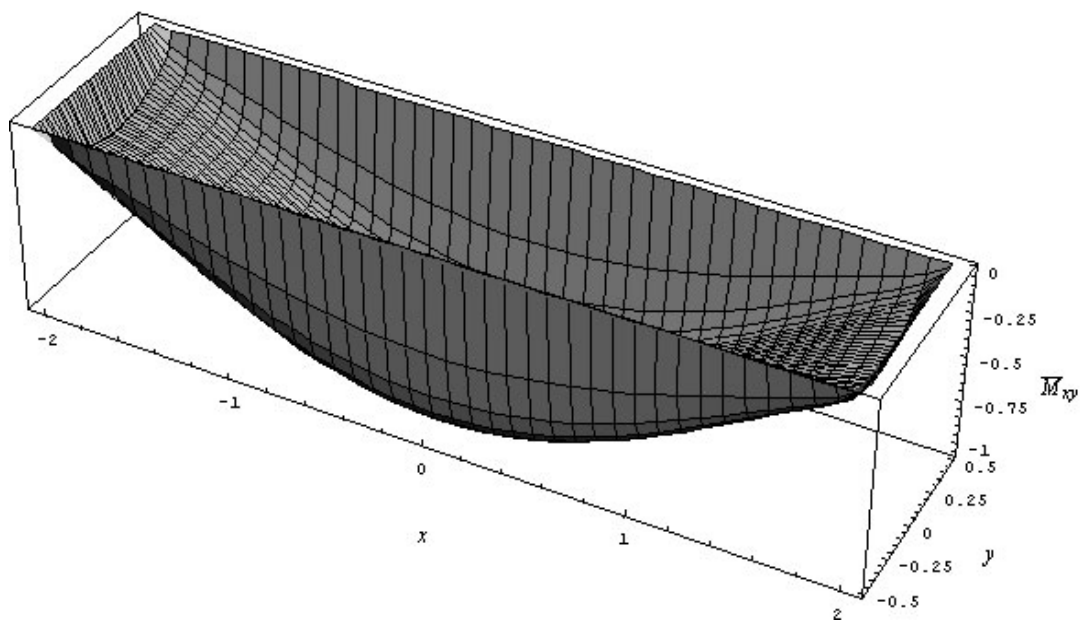

Fig. 9 (*continued*)

(b)

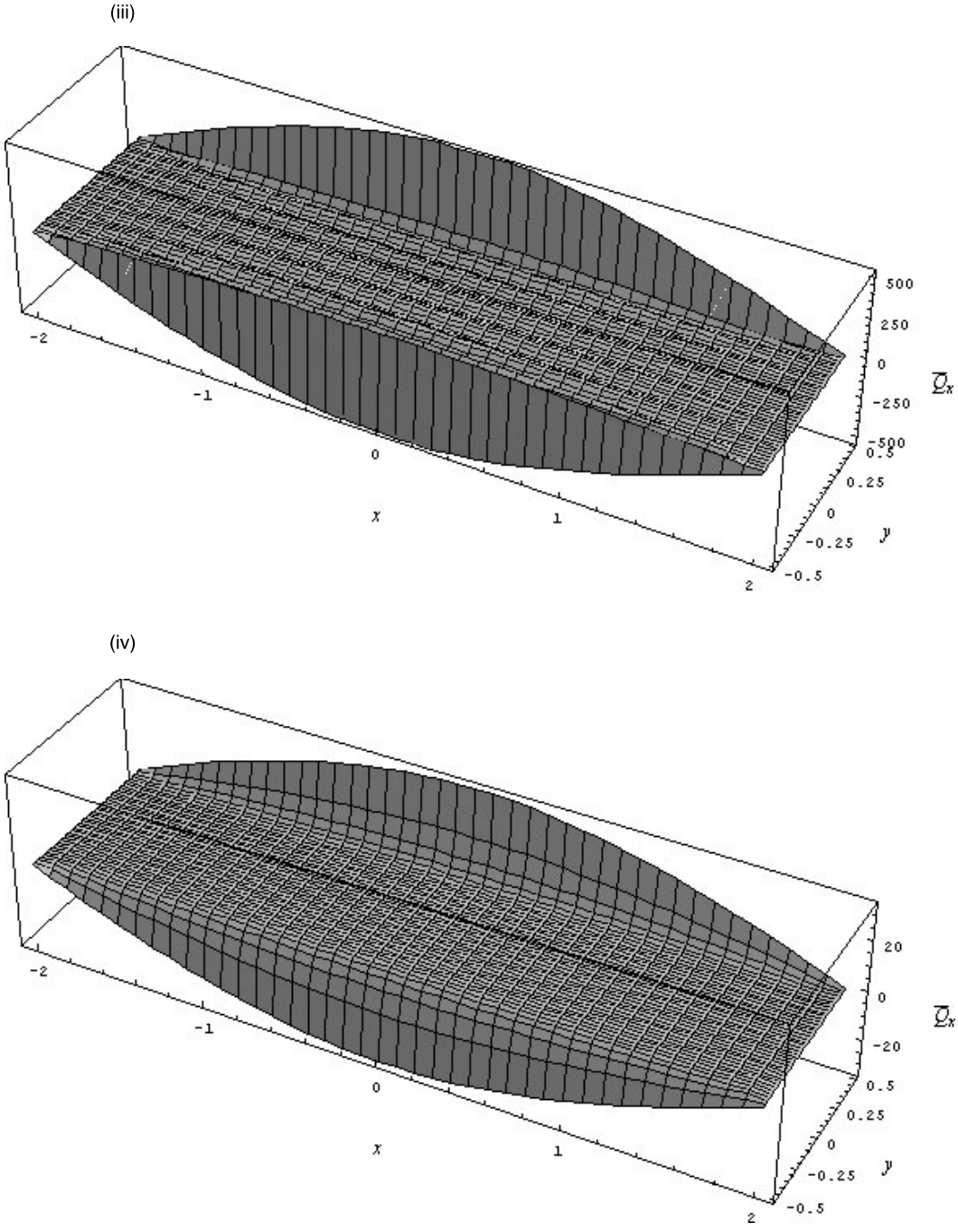

Fig. 9 (*continued*)

3. The modified Ritz method with a penalty functional (i.e. method C) does not speed up the convergence of the stress resultants, but it does ensure the satisfaction of the natural boundary conditions. For thin plates, it creates some distortions to the stress-resultant distributions and may need some special treatment to remove these undesirable effects.

4. Based on the numerical results of this paper, the Ritz method is more computationally efficient than the finite element method in determining the stress-resultant distributions in freely vibrating rectangular plates.

Acknowledgements

The first author is very grateful to Professor Eiichi Watanabe for the invitation to visit the Structural Engineering Laboratory of Kyoto University and to conduct this joint research work on floating structures. The financial assistance provided by the Japan Society for the Promotion of Science (JSPS) is greatly appreciated. The authors also wish to thank Mr Lim Goy Teck, National University of Singapore for his assistance in plotting Figs. 3–9.

References

Kant, T., Hinton, E., 1983. Mindlin plate analysis by segmentation method. J. Engng. Mech. ASCE 109 (2), 537–556.

Kashiwagi, M., 1998. A new solution method for hydroelastic problems of a very large floating structure in waves. 17th Int. Conference on Offshore Mech. Arctic Engng. ASME, OMAE98-4332, 1–8.

Liew, K.M., Wang, C.M., Xiang, Y., Kitipornchai, S., 1998. Vibration of Mindlin Plates: Programming the p-version Ritz Method, Elsevier, Oxford.

Mindlin, R.D., 1951. Influence of rotatory inertia and shear on flexural motion of isotropic elastic plates. ASME, J. Appl. Mech. 13, 31–38.

Nagata, S., Yoshida, H., Fujita, T., Isshiki, H., 1998. Reduction of the motion of an elastic floating plate in waves by breakwaters. In: M. Kashiwagi et al., (Eds.), Proceedings of the 2nd Hydroelasticity in Marine Technology, Kyushu University, Fukuoka, Japan, December 1–3, 1998, pp. 229–237.

Seto, H., Ochi, M., 1998. A hybrid element approach to hydroelastic behaviour of a very large floating structures in regular waves. In: M. Kashiwagi et al., (Eds.), Proceedings of the 2nd Hydroelasticity in Marine Technology, Kyushu University, Fukuoka, Japan, December 1–3, 1998, pp. 185–193.

Sim, I.H., Choi, H.S., 1998. An analysis of the hydroelastic behaviour of large floating structures in oblique waves. In: M. Kashiwagi et al., (Eds.), Proceedings of the 2nd Hydroelasticity in Marine Technology, Kyushu University, Fukuoka, Japan, December 1–3, pp. 195–199.

Xiang, Y., Wang, C.M., Kitipornchai, S., 1995. Fortran subroutines for mathematical operations on polynomial functions. Comp. Struct. 56 (4), 541–551.

Xiang, Y., Liew, K.M., Kitipornchai, S., 1997. Vibration analysis of rectangular Mindlin plates resting on elastic edge supports. J. Sound Vibration 204 (1), 1–16.

Utsunomiya, T., Watanabe, E., Eatock Taylor, R., 1998. Wave response analysis of a box-like VLFS close to a breakwater, 17th Int. Conference Offshore Mech. Arctic Engng. ASME, OMAE98-4331, pp. 1–8.